Viscosity and Crystallization in a Series of Zr-based Bulk Amorphous Alloys

Thesis by

Theodore A. Waniuk

In Partial Fulfillment of the Requirements

for the Degree of

Doctor of Philosophy

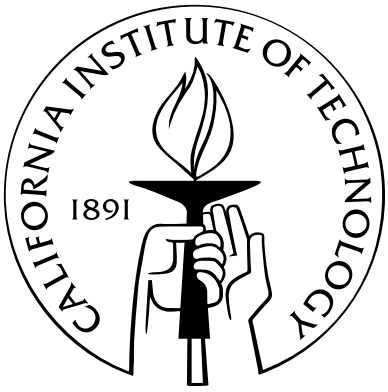

California Institute of Technology

Pasadena, California

2004

(Submitted May 28, 2004)

To Arianne

Acknowledgements

I would like to thank Professor Bill Johnson for allowing me to pursue my doctorate at the California Institute of Technology. His devotion to science and extraordinary insight have been a great boon, and I am grateful to have worked with him.

I am particularly thankful for the help offered by Ralf Busch and Jan Schroers. Their assistance made this work possible and my time at Caltech much more enjoyable. Considerable insight was also gained in fruitful discussions with Stephen Glade, Andreas Masuhr, Sven Bossuyt, Haein Choi-Yim, Dale Conner, and Channing Ahn. In addition, I would like to thank all the members of the Materials Science Option for helping to foster an atmosphere of friendliness and cooperation.

This research was made possible by the National Aeronautics and Space Administration (Grant No. NAG8-1744) and the Department of Energy (Grant No. DEFG-03-86ER45242).

Finally, my deepest thanks go to Kim Lumbard, whose wisdom helped me to overcome perceived obstacles, and Arianne Silva, whose care and support have been invaluable.

Abstract

The various influences on glass-forming ability and crystallization in a series of alloy compositions ranging along a tie-line from $Zr_{41.2}Ti_{13.8}Cu_{12.5}Ni_{10}Be_{22.5}$ to $Zr_{46.75}Ti_{8.25}Cu_{7.5}Ni_{10}Be_{27.5}$ are studied using multiple techniques. Both the kinetic and thermodynamic aspects of crystallization are examined experimentally and used to explain why, in this series, thermal stability is greatest in those alloys with the poorest glass-forming ability. Overall, the investigations reveal that a single criterion like thermal stability or high viscosity is an insufficient indicator of the glass forming ability in certain complex bulk glass-forming systems. Instead, in these complex systems, multiple criteria must be combined to get a complete picture.

The equilibrium viscosity of $Zr_{41.2}Ti_{13.8}Cu_{12.5}Ni_{10}Be_{22.5}$ and three other alloys was determined for temperatures near the glass transition using three-point beam bending. The results of these measurements indicate that the alloys in this system are moderately strong liquids, and relaxation behavior is directly influenced by a chemical decomposition process which occurs in the supercooled liquid.

This decomposition process also appears to affect the crystallization behavior in the same series of alloys. Critical cooling rates were determined by observing crystallization upon cooling from the molten state with different rates, and these were

compared to thermal analysis performed under constant heating conditions. The latter measurements show that the supercooled liquid region is largest for compositions midway between the two endpoints; in contrast, the critical cooling rate increases continuously from 1.4 K/s to 28 K/s for each successive alloy in this series.

In order to examine the crystallization process more closely, low temperature time-temperature-transformation diagrams for the alloy series were measured during isothermal annealing of initially amorphous specimens. For all investigated alloys, a primary quasicrystalline phase forms at a rate which varies substantially with alloy composition. Describing the complicated influences on crystallization required not only the previous thermal analysis but also constant heating measurements and x-ray diffraction data obtained after various states of annealing.

Contents

List of Figures

List of Tables

Chapter 1

Introduction

1.1 Interest in Glass-Forming Ability

In the 1960s it was discovered that certain binary metallic systems could be forced to solidify without crystallizing if cooled with a rate of approximately 10^6 K/s [1]. Subsequent decades witnessed the development of numerous multicomponent alloys with cooling rates to form a glass ranging from 100 K/s to 1 K/s [2, 3, 4, 5], allowing such materials to be cast in bulk form, with dimensions on the order of centimeters. In general, it has been found that glass-forming ability (GFA) in these bulk metallic glasses (BMG) tends to increase as more components are added to each alloy composition, implying a "confusion principle" [6]. Increasing the components in an alloy system destabilizes competing crystalline phases which form during cooling, effectively frustrating the alloy's ability to crystallize by making the liquid phase more stable relative to the crystalline phases. Over time, the discovery of new and better glass formers has naturally prompted a search for comprehensive underlying rules that predict GFA based on common thermodynamic and kinetic properties of BMG compositions. In pursuit of these principles, heuristic predictive indicators have been

	η	D^*	ΔT	T_{rg}	ΔG_{l-x}
Relationship to Glass-Forming Ability	GFA↑ as $\eta \uparrow$	GFA↑ as $D^* \uparrow$	GFA↑ as $\Delta T \uparrow$	GFA↑ as $T_{rg} \uparrow$	GFA↑ as $\Delta G_{l-x} \downarrow$

Table 1.1: Predictive indicators of glass-forming ability.

examined in an attempt to characterize the underlying mechanism.

1.2 Predictive Indicators of Glass-Forming Ability

Recent analysis of multicomponent system with excellent glass-forming ability has yielded correlations between various thermophysical properties and GFA. Table 1.1 summarizes these correlations for certain parameters discussed in this work, and represents the current consensus for a wide range of glass-forming systems. The majority of the parameters listed in Table 1.1 show a positive correlation with GFA. GFA is quantified by R_c, the critical cooling rate for glass formation. R_c is obtained by directly measuring the minimum rate at which a molten sample can be cooled without crystallizing. Kinetic parameters such as the equilibrium viscosity, η, and fragility parameter, D^*, show that alloys which exhibit high viscosities through a wide temperature range tend to form glasses more readily. Experimental evidence has supported a positive correlation between ΔT and T_{rg}, the thermal stability and reduced glass transition temperature, respectively, and GFA. Finally, ΔG_{l-x}, the Gibbs free energy difference between the liquid and the solid state, has a direct influence on nucleation and thus the ability to bypass crystallization during cooling.

From a thermodynamic standpoint, bulk glass formers naturally exhibit character-

istics which indicate a low driving force for crystallization in the supercooled liquid. This low driving force reduces nucleation rates and therefore correspondingly improves GFA. Thermal analysis of metallic glasses, particularly the more stable ones, allows the specific heat capacity, c_p, and enthalpy of fusion, ΔH_f, to be determined as a function of temperature. Using these parameters, ΔG_{l-x} can be calculated and compared for the various glass-forming compositions. According to classical nucleation theory, the free energy barrier to the formation of a crystalline nucleus in a supercooled liquid can be represented by

$$\Delta G^* = \frac{16\pi \cdot (\gamma_{sl})^3}{3 \cdot (\Delta G_{l-x})^2} \tag{1.1}$$

where γ_{sl} represents the interfacial free energy between the solid and liquid. This parameter in turn influences the steady-state nucleation rate through

$$I_{ss} = A \cdot D \cdot \exp\left(-\frac{\Delta G^*}{k_B T}\right) \tag{1.2}$$

where A is a constant, D represents an effective diffusivity, and k_B is Boltzman's constant. From these equations, it is clear that the steady-state nucleation rate increases as ΔG_{l-x} increases. Experiments have confirmed that bulk GFA is correlated with smaller values of ΔG_{l-x} [7].

Despite an observed discontinuity in the specific heat at the glass transition, it is inaccurate to consider the glass transition a thermodynamic phase transition. T_g, the glass transition temperature, depends on the experimental heating or cooling

rate used during measurements, and thus kinetic parameters such as viscosity have a significant influence on the GFA of a particular system. Bulk glass formers generally exhibit high equilibrium viscosities over a large temperature range between the melt and the amorphous solid.

The temperature dependence of the equilibrium viscosity can be described by a fragility parameter, D^*. Low values of D^* are associated with low melt viscosities and large changes in kinetic properties near T_g (fragile liquids), while high D^* values correspond to high melt viscosities and small changes in kinetic properties (strong liquids) [8]. BMG alloys, with melt viscosities substantially higher than pure metals and a relatively uniform variation of equilibrium viscosity over a large temperature range near T_g, fall into the latter category. Such behavior has a distinct influence on crystallization by retarding the formation and growth of crystalline nuclei during cooling, resulting in better GFA overall.

To describe and predict the ability to bypass crystallization in supercooled alloys, Turnbull suggested a criterion which takes into account thermodynamic and kinetic factors involved in nucleation and growth [9]. He demonstrated that as

$$T_{rg} = \frac{T_g}{T_l} = \frac{\text{glass transition temperature}}{\text{liquidus temperature}} \rightarrow \frac{2}{3}$$

homogeneous nucleation in an alloy would be substantially suppressed, leading to BMG behavior. T_{rg} has been used to predict the GFA of a large number of glass-forming compositions, and seems well suited to simpler alloys.

However, among the more complex multicomponent bulk metallic glasses are sev-

eral "rogue" glasses with glass-forming abilities that do not fit the predictions of the Turnbull criterion [10]. For example, despite high experimentally determined values of T_{rg} for $Zr_{41.2}Ti_{13.8}Cu_{12.5}Ni_{10}Be_{22.5}$ [11], microstructural investigations have revealed a high density of nanocrystals after annealing at low temperatures in the vicinity of the glass transition in this alloy [12]. This implies a high nucleation rate, contradicting predictions based on T_{rg}. Multiple explanations have been posited to explain this behavior, including phase separation in the undercooled liquid [12], a linked-flux model of nucleation [13], and catastrophic nucleation [14].

$Zr_{41.2}Ti_{13.8}Cu_{12.5}Ni_{10}Be_{22.5}$ (Vit1) and $Zr_{46.75}Ti_{8.25}Cu_{7.5}Ni_{10}Be_{27.5}$ (Vit4) have been extensively studied over the last decade. In order to investigate correlations between the various parameters discussed above, the author has performed studies on a series of alloys spaced equally in composition from Vit1 to Vit4. Though these studies have shown that the alloys in the series each have a different critical cooling rate and thermal stability (represented by ΔT, the temperature interval between the glass transition and the onset of crystallization), they all demonstrate excellent GFA, enabling the same experimental techniques to be applied to their study. In the past, both R_c and ΔT have been interchangeably used to describe the relative GFA for a large number of metallic glass compositions from multiple alloy families. For the Vit1-Vit4 series described above, however, the thermal stability tends to decrease as the critical cooling rate decreases (i.e., the GFA increases), whereas indicators predict that GFA should decrease with the thermal stability. This apparent contradiction makes Zr-Ti-Cu-Ni-Be a favorable system to elucidate the various influences on GFA.

1.3 Thesis Overview

The present work will discuss the results of crystallization kinetics and flow behavior studies performed on seven alloys along the tie line in composition space between Vit1 and Vit4. The various influences on GFA will be examined together as a function of composition: timescales for crystallization, timescales for viscous flow, thermodynamic properties, thermal stability, and previous results concerning nucleation density will all be utilized. Crystallization studies will be summarized in the form of time-temperature-transformation (TTT) diagrams, and viscosity data obtained using beam bending methods will be presented for all alloys and discussed in the framework of the fragility concept. These data show that even though the alloys near Vit4 exhibit the slowest crystallization kinetics upon heating amorphous material, they also have the lowest equilibrium viscosities for the same temperature range, counter to expectations.

To assist in describing the crystallization pathways in this system, additional X-ray diffraction (XRD) measurements taken after isothermal anneals of varying duration will also be presented. These XRD data reveal that all the alloys form a metastable quasicrystalline primary phase prior to subsequent bulk crystallization events. The combined XRD studies and thermal analysis suggest a mechanism for the crystallization process in this alloy series.

References

[1] W. Clement, R. H. Willens, and P. Duwez. *Nature*, 187:869, 1960.

[2] A. Inoue, T. Nakamura, N. Nishiyama, and T. Masumoto. *Mater. Trans JIM*, 33:937, 1992.

[3] A. Inoue, T. Zhang, N. Nishiyama, K. Ohba, and T. Masumoto. *Mater. Trans. JIM*, 34:1234, 1993.

[4] A. Peker and W. L. Johnson. *Appl. Phys. Lett.*, 63:2342, 1993.

[5] N. Nishiyama and A. Inoue. *Mater. Trans. JIM*, 37:1531, 1996.

[6] A. L. Greer. *Nature*, 366:303, 1993.

[7] R. Busch, W. Liu, and W. L. Johnson. *J. Appl. Phys.*, 83:4134, 1998.

[8] C. A. Angell. *Science*, 267:1924, 1995.

[9] D. Turnbull. *Contemp. Phys.*, 10:473, 1969.

[10] K. F. Kelton. *Int. J. Non-Equilib. Process.*, 11:141, 1998.

[11] A. Masuhr, R. Busch, and W. L. Johnson. *Mater. Sci. Forum*, 269-272:779, 1998.

[12] S. Schneider, P. Thiyagarajan, and W. L. Johnson. *Appl. Phys. Lett.*, 68:493, 1996.

[13] K. F. Kelton. *Philos. Mag. Lett.*, 77:337, 1998.

[14] H. Assadi and J. Schroers. *Acta Mater.*, 50:89, 2002.

Chapter 2

Viscosity Determination

Equilibrium viscosity in bulk metallic glass forming alloys (hereafter referred to as BMG alloys) varies by fourteen orders of magnitude from temperatures above the liquidus to near the glass transition, hence no single technique can be used to measure this parameter throughout the entire temperature range. Recently, alloy systems with high thermal stability against crystallization have allowed multiple techniques, some previously used to study silicate glasses and polymers, to be applied to the measurement of viscosity in BMG alloys. Techniques that have been used to study BMG alloys in the molten state include the capillary flow method (in which the liquid flow rate is observed as it is drawn up into a capillary by surface tension and hydrostatic pressure [1]) and concentric cylinder rheometry (in which concentric cylinders with liquid between them are are rotated against one another to generate a torque signal proportional to the liquid viscosity [2]). Techniques that have been used to measure viscosity at low temperatures include parallel plate rheometry (which measures the deformation of a cylinder of material between two plates under an applied load [3, 4]) and three-point beam bending (which derives viscosity from the time-varying midpoint deflection of a beam supported at both ends with a point load

applied to its center [5]).

For this study, three-point beam bending was utilized to measure equilibrium viscosities in the vicinity of the glass transition, because the technique yields accurate results over a large temperature range. Vit1 was studied extensively in the temperature range between approximately 600 K and 700 K, and the measured data were combined with additional high temperature data obtained in separate studies in order to derive a mathematical description of the equilibrium viscosity over a large range of temperatures from the liquid to the amorphous state of this alloy.

Several other compositions, designated Vit1a ($Zr_{42.63}Ti_{12.37}Cu_{11.25}Ni_{10}Be_{23.75}$), Vit1b ($Zr_{44}Ti_{11}Cu_{10}Ni_{10}Be_{25}$), and Vit1c ($Zr_{45.38}Ti_{9.62}Cu_{8.75}Ni_{10}Be_{26.25}$), were also examined using the three-point beam bending technique. These alloys, together with Vit1 and Vit4, fall at equally spaced intervals on the tie line in composition space described by $(Zr_{37.5+2.5x}Ti_{62.5-2.5x})_{55}(Cu_{100-3x}Ni_{3x})_{41.25-1.25x}Be_{3.75+1.25x}$, from $x = 13$ to $x = 19$. Fig. 2.1 describes the alloy series using a pseudo-ternary diagram in which the sum of the Zr and Ti forms one axis and the sum of the Cu and Ni forms another. The pseudo-ternary diagram is annotated to describe the trends in concentration for the various elements in the series. The viscosities of Vit1(-b) and Vit1(-a), also shown on the diagram, were not measured; Chapter 3 will discuss these additional compositions. In addition, viscosity measurements of Vit1a, Vit1b, and Vit1c were performed over a more limited range of temperatures than for Vit1.

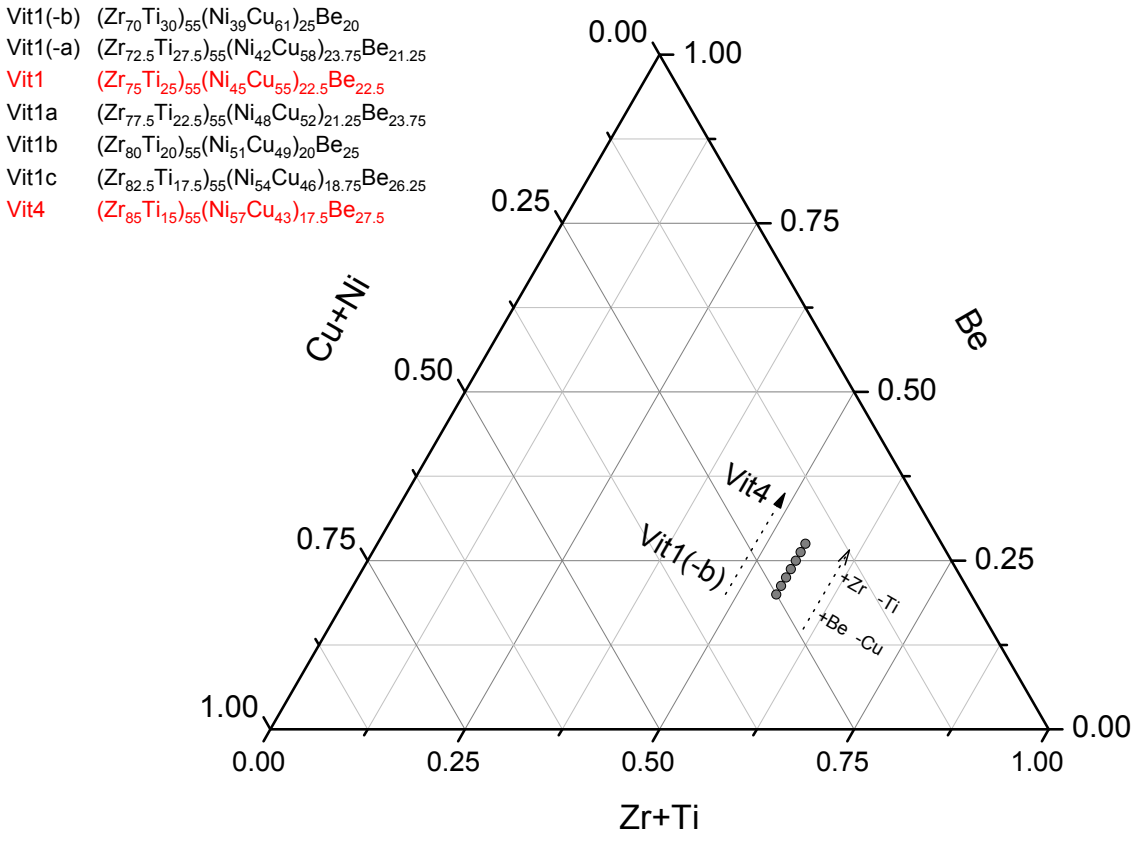

Figure 2.1: Pseudo-ternary diagram showing the alloy series (Vit1(-b) to Vit4) described by $(Zr_{37.5+2.5x}Ti_{62.5-2.5x})_{55}(Cu_{100-3x}Ni_{3x})_{41.25-1.25x}Be_{3.75+1.25x}$, from $x = 13$ to $x = 19$.

2.1 Setup and Technique

Samples of Vit1, Vit1a, Vit1b, and Vit1c were prepared with elements of 99.5% to 99.995% purity. The constituents were first arc-melted in a titanium-gettered argon atmosphere to produce a homogeneous ingot. They were then sealed in a quartz tube under a vacuum of 10^{-6} mbar, heated above the liquidus for 5 minutes, and subsequently quenched in water with a cooling rate of approximately 50 K/s to create fully amorphous samples. From these, beams with rectangular cross sections between 0.1 and 1.1 mm^2 and lengths of approximately 10 mm were cut. A Perkin-Elmer Thermal Mechanical Analyzer (TMA 7), calibrated using the melting points of indium and zinc standards, was used to conduct isothermal measurements of viscosity. In addition, differential scanning calorimetry (DSC) was used to observe enthalpy relaxation and crystallization in these alloys. Samples were subjected to isothermal anneals and 20 K/min heating rates in a Perkin Elmer DSC 7, which recorded phase changes during the experiments.

The three-point beam bending apparatus is shown schematically in Fig. 2.2. This technique involves the application of a load to the center of a beam with uniform cross section, supported at both ends. Under isothermal test conditions, the deflection of the center of the sample under a constant load is measured over time and used to calculate the time-dependent viscosity. Viscosity values are obtained from the deflection data using the following equation [5, 6, 7]:

$$\eta = -\frac{gL^3}{2.4I_c v}\left(M + \frac{\rho AL}{1.6}\right) \tag{2.1}$$

where

η is the viscosity in Pa s,

g is the gravitational constant (m/s^2),

I_c is the cross sectional moment of inertia (m^4),

v is the midpoint deflection velocity (m/s, $v<0$),

M is the applied load (kg),

ρ is the density of the material (kg/m^3),

A is the cross sectional area of the beam (m^2), and

L is the support span (5.08×10^{-3} for this setup).

Viscosities between 10^7 and 10^{14} Pa s can be measured with this technique, allowing the amorphous alloy, the glass transition region, and the deeply supercooled liquid of $Zr_{41.2}Ti_{13.8}Cu_{12.5}Ni_{10}Be_{22.5}$ and similar alloys to be explored.

A typical viscosity measurement proceeded as follows: a beam was aligned on the two supports, the probe was lowered, and the load was applied at ambient temperature. Then, the apparatus was placed in a furnace and heated at a rate of 200 K/min under a flow of high purity helium gas until the isothermal annealing temperature was reached. After the sample reached the annealing temperature, relative deflection of the center of the beam downward was recorded. In order to obtain a value for equilibrium viscosity at this annealing temperature, the time derivative of the deflection signal was calculated and applied to Eq. 2.1 for each sample.

The experimental apparatus allowed a total range of displacement of 1 mm during beam bending. For each experiment, the cross section of the beam and the applied

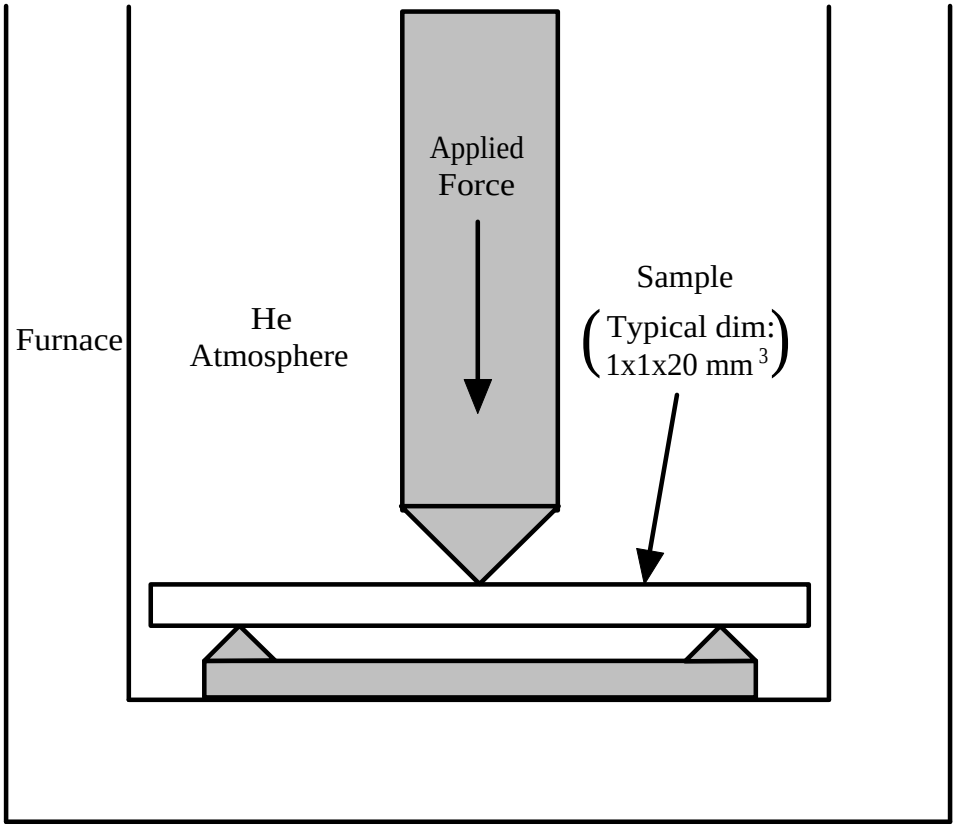

Figure 2.2: Schematic representation of three-point beam bending setup.

force were selected to yield results which maximized the total deflection without exceeding 1 mm. These selection criteria were necessary to increase the signal to noise ratio of the resulting data, a critical factor for minimizing scatter when the viscosity changed by several orders of magnitude during long-duration measurements. At low temperatures in particular, it became difficult to analyze the data as scatter overwhelmed the general trend. This occurred because the deflection signal changed very slowly with time, and the changes were on the order of the increment of distance that is detectable by the equipment. In order to analyze low temperature measurements with excessive scatter, the data were smoothed using a parabolic FFT clipping function with cutoff frequency $\frac{1}{n\Delta t}$ (n is the number of points considered, t is the time interval between successive points). Fig. 2.3 shows an example of viscosity data smoothed using this technique.

2.2 Results

Fig. 2.4 shows deflection data obtained by beam bending during annealing at 643 K for 16000 s. The deflection rate is initially large and decreases in magnitude during the testing period. When substituted into Eq. 2.1, the viscosity data can be calculated as depicted in Fig. 2.4. Here, the measured deflection of the sample corresponds to an increase of the viscosity over time. It is apparent from these data that the viscosity increase in Vit1 occurs in two stages: a primary, rapid increase of viscosity by approximately a factor of two for short times up to 1000 s, and a secondary rise that continues for much longer times and leads to a change of viscosity of about two

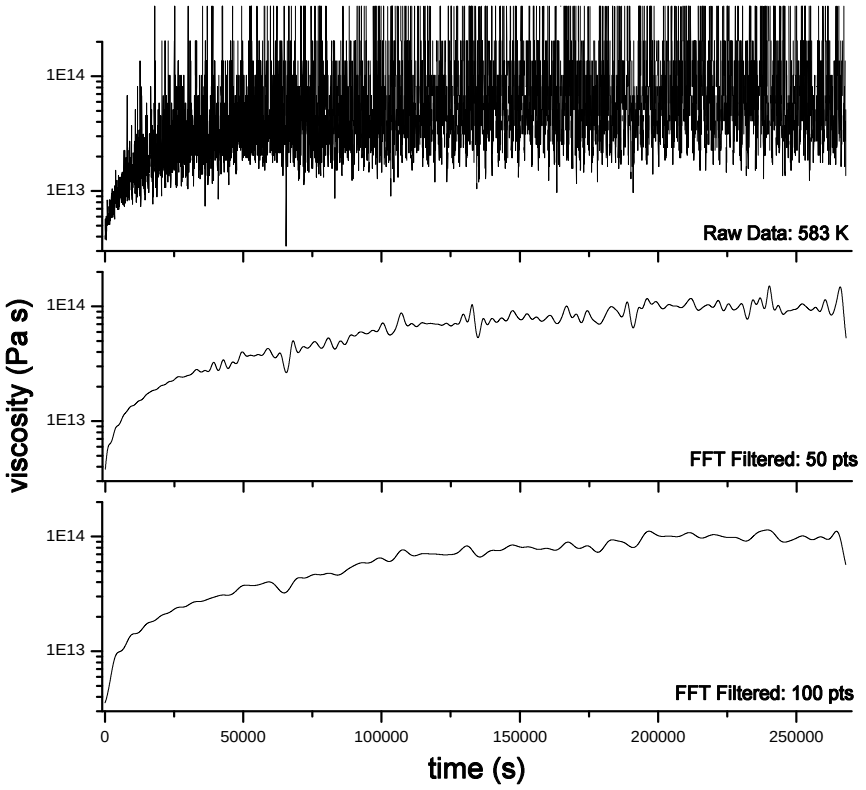

Figure 2.3: Viscosity data smoothed using a FFT clipping function. Frequencies higher than $\frac{1}{n\Delta t}$, where n is the number of points considered and t is the time interval between points, were removed in the lower two graphs.

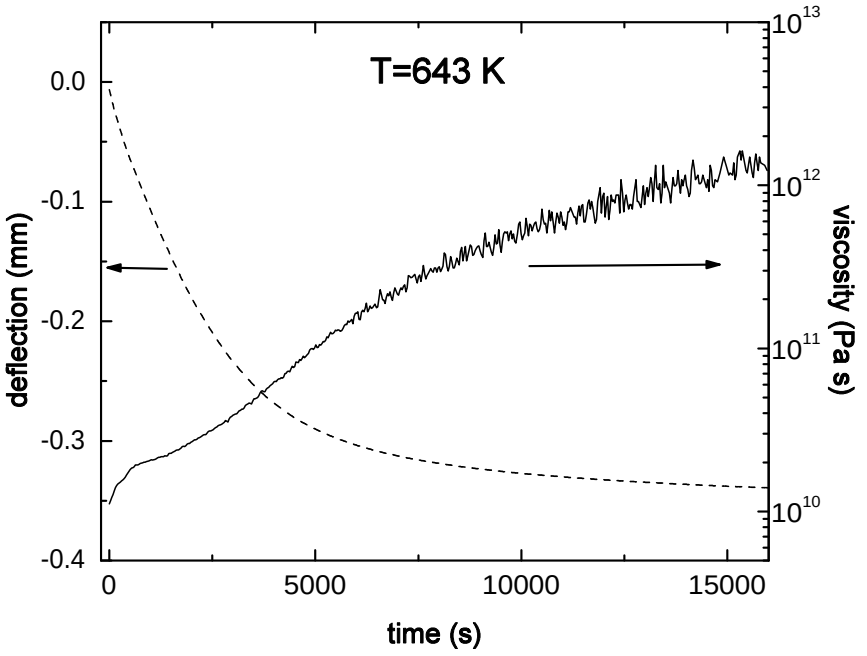

Figure 2.4: Deflection data and calculated viscosity data obtained during annealing at 643 K.

orders of magnitude within the shown time frame.

Isothermal viscosity data for 618 K, 638 K, and 653 K are plotted in Fig. 2.5. Measurements at these temperatures also show an increase in viscosity which proceeds in two stages. Significant deviations from the initial viscosity change begin to be observed at the times marked by arrows, and these times become shorter with increasing annealing temperature. Fits to the initial relaxation are also included in Fig. 2.5; the technique used to fit the curves will be explained in Section 2.3.1 of this chapter.

For higher annealing temperatures, the timescale for relaxation of the amorphous phase is much shorter. Fig. 2.6 contains data taken at 663 K. Unlike the measurements shown in Figs. 2.4 and 2.5, these data display no notable upward relaxation

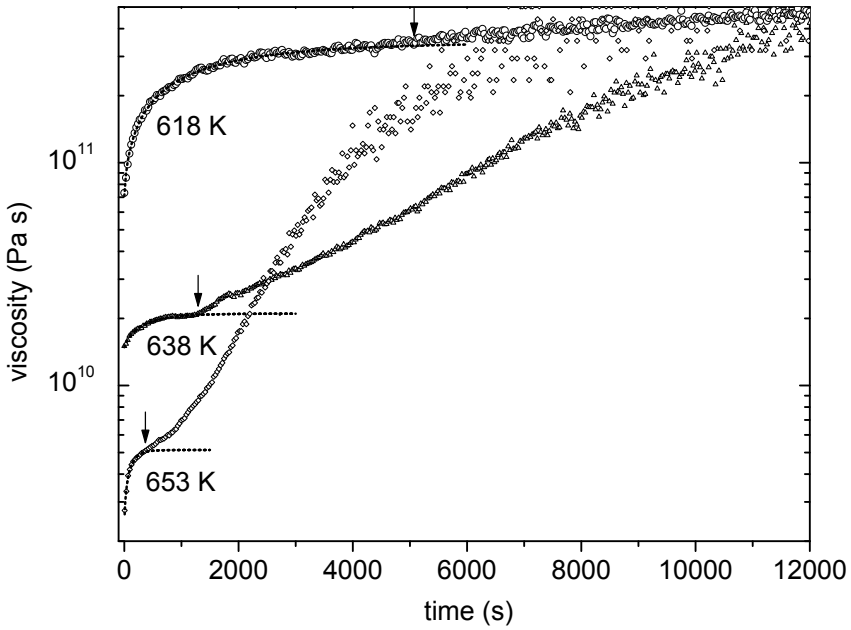

Figure 2.5: Isothermal viscosity measurements at three different temperatures. The initial increase in viscosity is fitted by a stretched exponential function and represents an isothermal relaxation from the amorphous state into the supercooled liquid. Arrows at each curve indicate deviation from the initial relaxation.

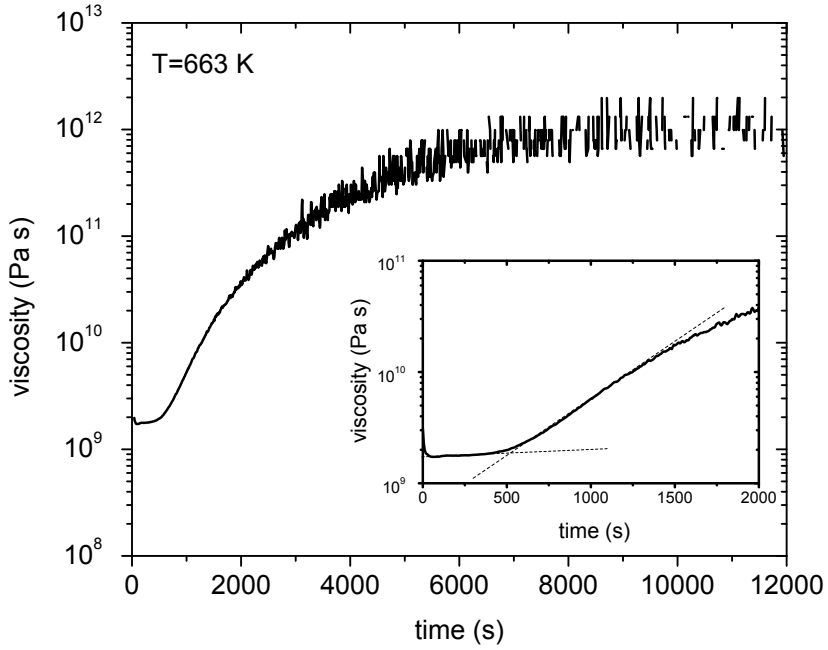

Figure 2.6: Isothermal viscosity measurement at 663 K. Deviations from the equilibrium viscosity are observed after 500 s (inset).

in the beginning of the measurement, because the relaxation time at an equilibrium viscosity of 2×10^9 Pa s is only a few seconds. With such a short relaxation time, the viscosity is constant immediately after the annealing temperature is reached. Considerable deviations from the equilibrium viscosity of the original alloy are observed after 500 s at 663 K (see inset of Fig. 2.6), and the material undergoes a viscosity change of almost three orders of magnitude from 2×10^9 to 1.3×10^{12} Pa s between approximately 500 and 8000 s. For longer times, the viscosity remains constant, suggesting that a metastable equilibrium state has been reached. Figs. 2.4-2.6 suggest that, for a wide range of test temperatures, drastic changes in the alloy's structure or composition occur over the course of each isothermal measurement, resulting in a tremendous increase of viscosity with time.

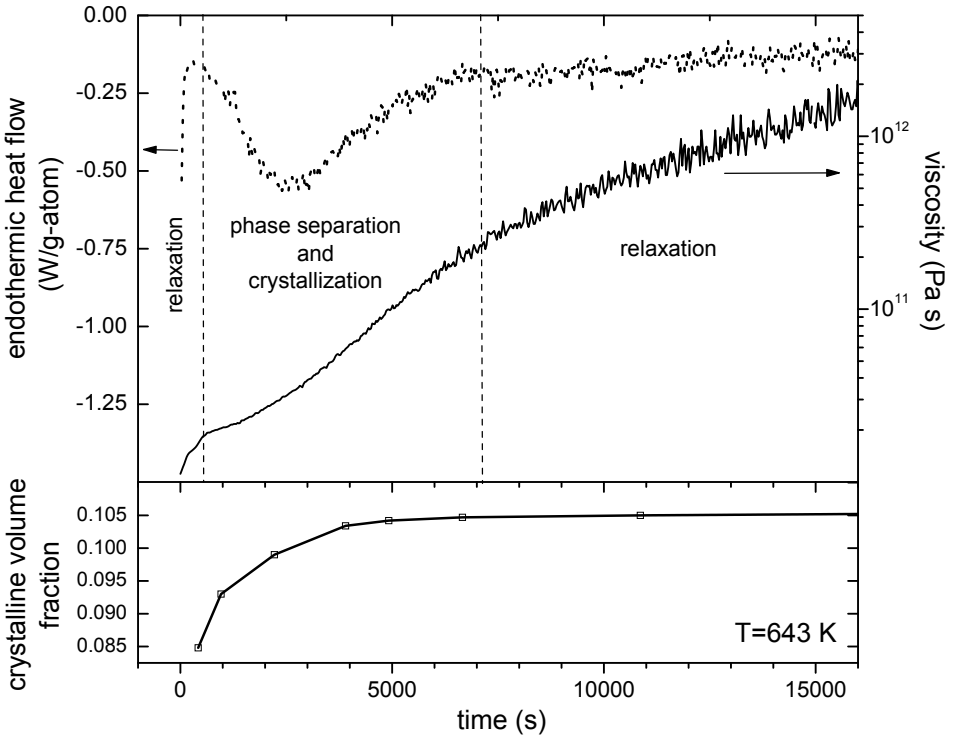

Figure 2.7: Isothermal DSC scan, viscosity measurement, and volume fraction of nanocrystals [8] at a temperature of 643 K.

In addition to the rheological measurements, DSC was employed to observe enthalpy relaxation and crystallization in $Zr_{41.2}Ti_{13.8}Cu_{12.5}Ni_{10}Be_{22.5}$ during isothermal annealing at several temperatures. Fig. 2.7 compares the DSC results with viscosity changes at 643 K. In the DSC scan, the initial rise corresponds to enthalpy relaxation of the alloy, during which quenched-in free volume heals out. This process is reflected in the initial increase of the viscosity. Subsequently, an exothermic peak is observed in the DSC curve. This peak is caused by phase separation and primary crystallization of the alloy and has a direct effect on the viscosity change of the alloy, causing a shift to a much higher viscosity at a given temperature. The crystalline volume fraction data depicted in the lower part of Fig. 2.7 will be discussed in Section 2.3.2.

2.3 Discussion

2.3.1 Equilibrium Viscosity

In order to determine the equilibrium viscosity of the initially homogeneous alloy, relaxation from the amorphous state into the supercooled liquid has to be considered. For Vit4, it was shown that in the respective temperature interval around the glass transition the viscosity relaxation can be described by a single stretched exponential function [9],

$$\eta(t) = \eta_a + \eta_{eq-a}(1 - e^{-(t/\tau_S)^\beta}) \tag{2.2}$$

where

τ_S is an average shear relaxation time,

β is a stretching exponent of the order of 0.8,

t is the time,

η_a is the viscosity of the alloy before relaxation, and

η_{eq-a} is the total viscosity change during relaxation from the amorphous state into the supercooled liquid.

In contrast to Vit4, the viscosity changes of Vit1 during the course of the present experiments cannot be described by one stretched exponential function, as phase separation and partial crystallization have to be considered. However, the first relaxation event can be reasonably well characterized by Eq. 2.2. Using this relationship, the viscosity data have been fitted to determine the equilibrium viscosity as a function of temperature for the chemically homogeneous alloy before phase separation and

crystallization have progressed.

Fig. 2.8 summarizes the viscosity data for Vit1 as a function of temperature. Below 658 K the equilibrium viscosities of the quasi-homogeneous alloy are obtained by fitting the first relaxation event to Eq. 2.2. The equilibrium values above 658 K are determined from the experiments by taking the constant viscosity value directly after reaching the annealing temperature (see Fig. 2.6). Fig. 2.8 also shows the viscosity values that are reached after partial crystallization of the sample has occurred. The latter data are evaluated from the effective upper viscosity limit of the second viscosity change for 643-673 K (for example, the average viscosity between 8000 and 12000 s in Fig. 2.6) and are not determined from fits to Eq. 2.2. This equation is not applicable because the viscosity increase is caused by a combination of phase separation, nanocrystal formation, composition redistribution, and relaxation. We discuss this in more detail in Section 2.3.2.

To describe the temperature dependence of the equilibrium viscosity in the entire range of beam-bending data depicted in Fig. 2.8, the Vogel-Fulcher-Tammann (VFT) relation [10]

$$\eta(T) = \eta_0 \cdot \exp \frac{D^* \cdot T_0}{(T - T_0)} \tag{2.3}$$

is used, where

η_0 is set to $4{\times}10^{-5}$ Pa s [11]

D^* is the fragility parameter, and

T_0 is the VFT temperature, typically used as a fitting parameter.

The VFT fit also includes data obtained from the molten liquid near 1000 K using

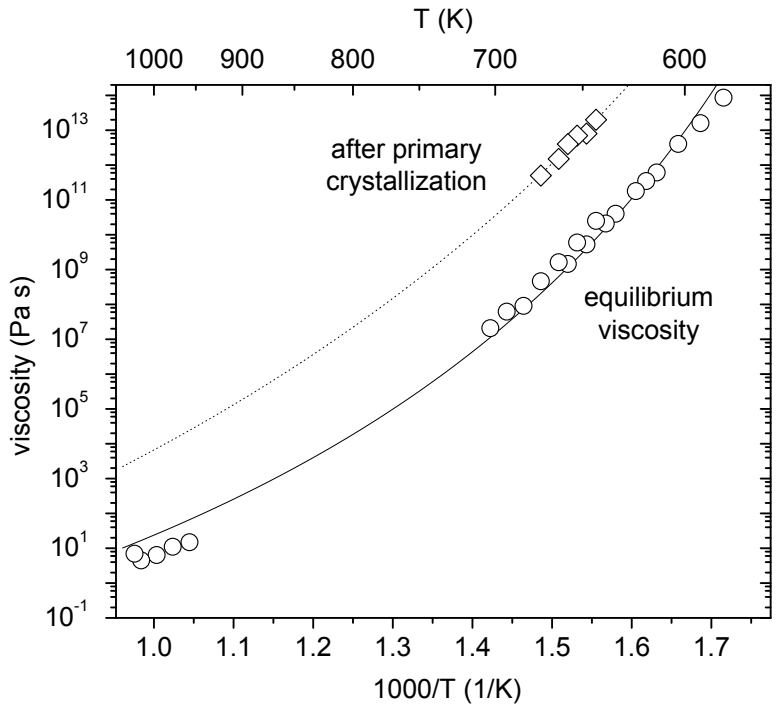

Figure 2.8: Equilibrium viscosity of Vit1 before and after primary crystallization.

rotating concentric cylinder experiments [2, 12], and yields $D^* = 18.5$ and $T_0 = 412.5$. Similar fragility parameters were found for $Zr_{46.75}Ti_{8.25}Cu_{7.5}Ni_{10}Be_{27.5}$ [9] and $Mg_{65}Cu_{25}Y_{10}$ [13].

In Fig. 2.9 the viscosity of Vit1 is compared with three non-metallic glass formers in a fragility plot. In this plot the viscosity data are normalized to a temperature where all the materials exhibit the same relaxation time (or viscosity). This temperature, T_g^*, is chosen as the temperature where the supercooled liquids exhibit a viscosity of 10^{12} Pa s. Within the framework of the fragility concept, liquids whose viscosities exhibit Ahrrenius behavior and remain very high in the molten state, such as SiO_2, are termed strong liquids. Fragile liquids, in contrast, have low melt viscosities and exhibit a dramatic change in viscosity close to T_g^*. According to Fig. 2.9,

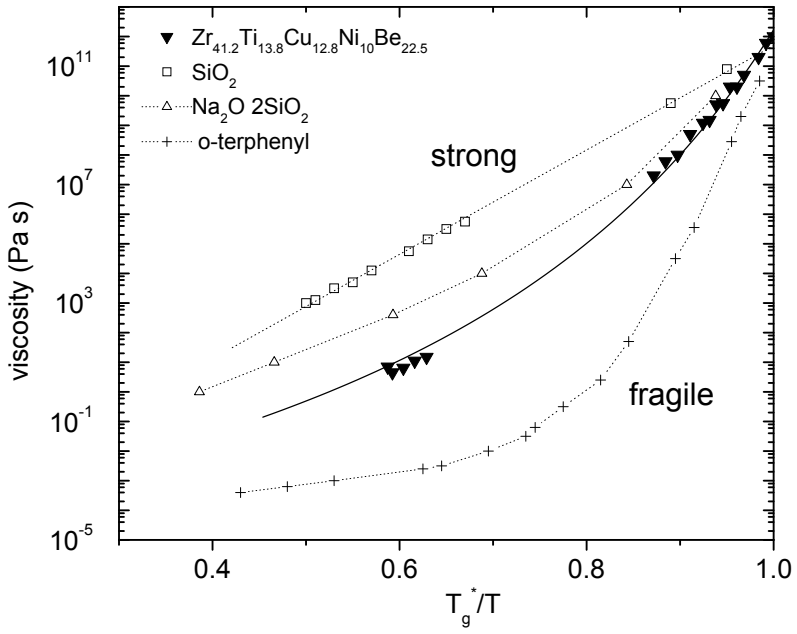

Figure 2.9: Fragility plot of the viscosities of Vit1 and three non-metallic glasses (Ref. [10]).

Vit1 is a moderately strong liquid, exhibiting behavior similar to that of Na_2O $2SiO_2$. This is consistent with the high melt viscosity of the order of 10 Pa s observed in this metallic glass-forming alloy (measured melt viscosities are included in Fig. 2.9). For further discussion on the strong liquid behavior of bulk metallic glass-forming liquids, see Refs [9, 13].

Viscosity data obtained for all the alloys in the series between Vit1 and Vit4 are shown in Fig. 2.10. Also included on the plot are the various techniques used to obtain the viscosity values at both high and low temperatures. From these data, it appears that the equilibrium viscosities of Vit1a, Vit1b, and Vit1c lie between those of Vit1 and Vit4 in the low-temperature regime. In addition, Vit1c exhibits lower equilibrium viscosity values than the other two alloys in the limited temperature range studied.

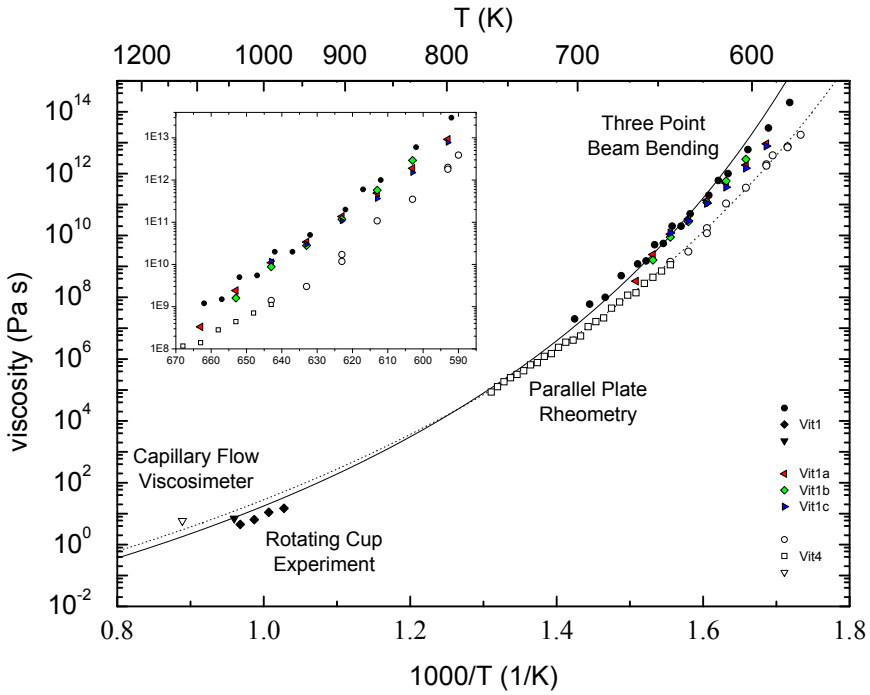

Figure 2.10: A summary of the results of equilibrium viscosity measurements for Vit1-Vit4.

Fitting the data for Vit1a, Vit1b, and Vit1c using Eq. 2.3 yields D* values of 21.3, 18.9, and 25.9, respectively. The data for Vit4 were obtained in a previous study by Bakke et al. [14], and a VFT fit to those data yielded a value of 22.7. The error in D* due to the fitting process for the three middle alloys is approximately ±1.3, though the small number of points combined with the lack of high-temperature data for these alloys increases the overall error relative to Vit1 and Vit4. The following subsection focuses on the changes in apparent viscosity during the phase transformations that occur in Vit1 close to the glass transition. The other alloys in the series are examined in more detail in the chapters that follow.

2.3.2 Effect of Phase Changes on Flow

As noted earlier, the viscosity data obtained from Vit1 during isothermal beam bending experiments cannot be described by Eq. 2.2 for the entire duration of each measurement. Rather than following stretched exponential behavior, the viscosity sometimes varies in multiple stages, reaching two distinct plateaus. At temperatures where the material is in the supercooled liquid state directly after reaching the annealing temperature (above 658 K, using a heating rate of 0.833 K/s to reach the annealing temperature), the viscosity in the isothermal experiment first stays constant (see Fig. 2.6). Then, a large increase of viscosity over several orders of magnitude occurs until a second steady state is observed. For lower temperatures (Figs. 2.5 and 2.7) the samples first show typical stretched exponential relaxation toward the equilibrium state until changes in the material begin to cause deviations from this behavior. The DSC thermogram depicted in Fig. 2.7 helps explain this phenomenon. Prior studies have shown that primary crystallization in Vit1, evidenced by the exothermic event depicted at the top of Fig. 2.7, is not the result of homogeneous nucleation from the supercooled liquid state [15], but is instead the result of nanocrystallization following composition fluctuations that likely proceed through a spinodal phase separation process.

Evidence of phase separation and nanocrystallization after heat treatment close to the glass transition in Vit1 has been previously provided by Schneider et al. [16, 17], and Liu et al. [8]. In the former, small angle neutron scattering (SANS) experiments showed that the phase separation process has a critical temperature of approx-

imately 671 K. Below this temperature, composition fluctuations with a temperature-dependent characteristic wavelength are generated within the amorphous alloy during annealing, indicative of a spinodal process. These quasi-periodic fluctuations in composition increase in amplitude until the crystallization temperature in certain phase-separated domains approaches the annealing temperature. Thus, after a certain period of time the barrier to nucleation of nanocrystals decreases, and nanocrystals form on a spatially correlated length scale.

Additional SANS experiments conducted by Liu et al. [8] confirm the previous description of phase separation in Vit1. If nanocrystallization follows phase separation, a small volume fraction of crystalline material should be present after a certain temperature-dependent annealing time. From the scattering data, the volume fraction of precipitates vs. annealing time is estimated in the Liu study for several temperatures. These volume fraction data are shown in the lower portion of Fig. 2.7 for a temperature of 643 K. Given TEM [16] and DSC results, we believe the data represent the volume fraction of a crystalline phase that forms in one set of phase separated domains. Ref. [8], in contrast, assumes the phases that contribute to the SANS signal are non-crystalline. It can be seen from Fig. 2.7 that the crystalline volume fraction initially increases rapidly in the same time interval where the pronounced DSC crystallization peak and the deviations of the viscosity from equilibrium are observed. The volume fraction reaches a value of approximately 0.105 at about 5000 s. Despite this relatively low volume fraction, the viscosity changes by nearly one order of magnitude during precipitation and continues to climb even after the crystalline

volume fraction reaches a constant value with time.

In order to quantify the effect of the nanocrystals on the viscosity change, a correction according to Einstein's equation for the flow of mixtures [18] can be made to the equilibrium viscosity obtained from the first relaxation event. This correction accounts for the viscosity change due to a small volume fraction of spherical particles suspended in a medium of known viscosity. In the equation

$$\eta_{eff} = \eta(1 + 2.5\xi) \tag{2.4}$$

η_{eff} is the viscosity of the mixture, η is the viscosity of the surrounding medium, and ξ is the volume fraction of particles. According to Eq. 2.4, a crystalline volume fraction of 0.105 would cause a shift of less than 30% in the effective viscosity of Vit1 if the viscosity of the surrounding medium is assumed the same before and after particles are added. Experimental observations show an increase in viscosity of about three orders of magnitude subsequent to the the initial relaxation of the quasi-homogeneous alloy. Therefore, the equilibrium viscosity of the non-crystalline matrix itself must have changed significantly. Since polyamorphism (where a supercooled liquid decomposes into two liquids with the same composition but different densities and fragilities [19]) is unlikely to be observed in a metallic liquid, the matrix must have changed to a composition with a higher equilibrium viscosity at a given annealing temperature.

In Fig. 2.7, both the volume fraction increase and the crystallization peak in the DSC scan reveal a crystallization event that begins shortly after the start of measurement and ends approximately 6000 s later. The second viscosity increase,

however, continues for much longer times. This suggests that, following the effective end of primary crystallization, further changes in viscosity are caused by concentration redistribution and relaxation of the non-crystalline matrix surrounding the nanocrystals. In order to investigate this effect, constant heating rate (20 K/min) DSC thermograms were obtained for the initially homogeneous alloy and also for the matrix after annealing for two different durations. These data are shown in Fig. 2.11. The onset of the calorimetric glass transition of the as-prepared sample is observed at approximately 625 K. After annealing, the glass transition has shifted to higher temperatures and the glass transition region has broadened. Because the kinetic glass transition reflects the relaxation time and the temperature dependence of the viscosity in the supercooled liquid [9], the shift of T_g in the matrix to higher temperatures is consistent with the increase in viscosity of the matrix after primary crystallization. With increasing annealing time prior to the DSC scan, the first exothermic peak, caused by phase separation and primary crystallization, vanishes. After the sample has been annealed for 6000 s, the approximate time at which the crystal volume fraction increase has ceased, the subsequent DSC scan only shows a small exothermic effect which can be attributed to growth of the primary nanocrystals before the remaining matrix crystallizes during secondary crystallization. After annealing for 54000 s, the DSC scan shows no evidence of nanocrystal growth, indicating that a metastable equilibrium state has been reached. The glass transition has shifted to an even greater temperature.

A VFT fit to the effective equilibrium viscosity data recorded after the end of

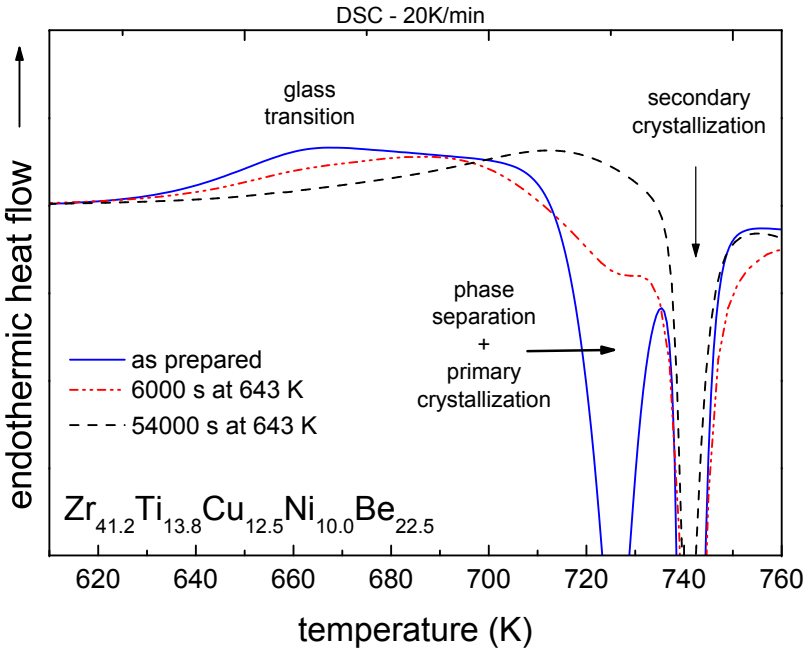

Figure 2.11: DSC scans of Vit1 as-prepared (solid line), after annealing at 643 K for 6000 s, and after annealing at 643 K for 54000 s.

primary crystallization, shown in Fig. 2.8, yields a higher D^* than the initially homogeneous alloy. Despite the fact that the final state of the alloy consists of nanocrystals embedded in an amorphous matrix, such a fit is justified owing to the negligible change in viscosity caused by nanocrystal formation. The formation of nanocrystals causes, according to Eq. 2.4, a viscosity change in an otherwise uniform matrix of less than a factor of two; such a small change can be neglected when compared to viscosity changes of three orders of magnitude. The VFT fit therefore primarily describes the viscosity of the final matrix, and it reveals that the matrix after phase separation and local primary crystallization is, overall, a stronger liquid than homogeneous Vit1. This, in turn, implies that the remaining amorphous material surrounding the nanocrystals is possibly a better glass former than the original homogeneous alloy.

To summarize, the viscosity of Vit1, Vit1a, Vit1b, and Vit1c was measured in the supercooled liquid and amorphous states. These alloys show strong liquid behavior, and phase changes in the samples during testing contribute to modified stretched exponential behavior with multiple relaxation events. After relaxation during annealing, the viscosity of Vit1 appears to increase significantly. This unusual behavior is attributed to phase separation which precedes nanocrystal formation.

References

[1] E. W. Washburn. *Phys. Rev.*, 17:273, 1921.

[2] A. Masuhr. *Viscous Flow and Crystallization of Bulk Metallic Glass Forming Liquids*. PhD thesis, California Institute of Technology, 1999.

[3] S. J. Wilson and D. Poole. *Mat. Res. Bull.*, 25:113, 1980.

[4] G. J. Diennes and H. F. Klemm. *J. Appl. Phys.*, 17:458, 1946.

[5] H. E. Hagy. *J. Am. Ceram. Soc.*, 46:93, 1963.

[6] F. T. Trouton. *Proc. R. Soc. A*, 77:426, 1906.

[7] M. Reiner. *Rheology*, volume 1, page 9. Academic Press, New York, 1956.

[8] J. M. Liu, A. Wiedenmann, U. Gerold, U. Keiderling, and H. Wollenberger. *Phys. Stat. Solidi B*, 199:379, 1997.

[9] R. Busch, E. Bakke, and W. L. Johnson. *Acta Mater.*, 46:4725, 1998.

[10] C. A. Angell. *Science*, 267:1924, 1995.

[11] S. V. Nemilov. *Glass Phys. Chem.*, 21:91, 1995.

[12] R. Busch, A. Masuhr, E. Bakke, and W. L. Johnson. *Mater. Res. Soc. Symp. Proc.*, 455:369, 1997.

[13] R. Busch, W. Liu, and W. L. Johnson. *J. Appl. Phys.*, 83:4134, 1998.

[14] E. Bakke, R. Busch, and W. L. Johnson. *Mater. Sci. Forum*, 225:95, 1996.

[15] R. Busch, E. Bakke, and W. L. Johnson. *Mater. Sci. Forum*, 235-238:327, 1997.

[16] S. Schneider, P. Thiyagarajan, and W. L. Johnson. *Appl. Phys. Lett.*, 68:493, 1996.

[17] S. Schneider, U. Geyer, P. Thiyagarajan, and W. L. Johnson. *Mater. Sci. Forum*, 235-238:337, 1997.

[18] A. Einstein. *Ann. Phys.*, 34(4):592, 1911.

[19] C. A. Angell, P. H. Poole, and J. Shao. *Il Nuovo Cimento*, 16:993, 1994.

Chapter 3

Thermal Analysis: Constant Cooling and Heating

The correlation in metallic glass forming systems between GFA, represented by the critical cooling rate (R_c) and the reduced glass transition temperature (T_{rg}) has been confirmed in many experiments (see, for example, Ref. [1]). However, R_c is generally difficult to measure directly, and therefore other criteria have been used to indicate relative GFA. For some systems it has been demonstrated that larger values of ΔT, usually quantified by measuring the temperature difference between the glass transition and the first crystallization event upon heating at a constant rate, tend to be associated with lower values of critical cooling rate. As a result, the thermal stability, represented by ΔT, has also served as an indicator of GFA in some alloy systems.

In recent years, the crystallization of Vit1 has been extensively examined [2, 3, 4, 5]. The tendency of this alloy to undergo chemical decomposition in the supercooled liquid [2, 3, 4] has a direct influence on the subsequent nucleation and growth of crystalline phases. Evidence of a chemical decomposition process has also been

observed in Vit1a, Vit1b, and Vit1c [6]. Since the decomposition occurs at temperatures close to T_g, the isothermal crystallization behavior of Vit1 for low supercooling is quite different from its behavior when deeply supercooled [5]. In addition, a study by Schroers et al. [7] involving constant heating and cooling experiments has shown that Vit1 crystallizes in a different manner upon heating from the amorphous solid than upon cooling from the melt. In that study, a cooling rate of approximately 1 K/s was required to bypass crystallization during cooling, whereas a heating rate of 200 K/s was necessary to avoid crystallization of a detectable volume fraction.

This chapter details the results of two series of experiments performed on Vit1, Vit1a, Vit1b, Vit1c, Vit4, and two additional alloys, $Zr_{39.88}Ti_{15.12}Cu_{13.77}Ni_{9.98}Be_{21.25}$ (Vit1(-a)), and $Zr_{38.5}Ti_{16.5}Cu_{15.25}Ni_{9.75}Be_{20}$ (Vit1(-b)). First, the critical cooling rate R_c was measured directly by melting alloy samples and subsequently cooling them at multiple controlled rates until crystallization occurred. Second, the alloys were examined during heating at a constant rate from the amorphous state to the molten state. These experiments resulted in the determination of several quantities, R_c, ΔT, and T_{rg}, used to quantify GFA. R_c is compared directly with ΔT and T_{rg} values for each alloy.

3.1 Setup and Technique

Alloy samples were prepared in the same manner as described in Chapter 2. A Perkin Elmer differential thermal analyzer (DTA 7) was used for continuous heating measurements. Samples were heated at 10 K/min in order to determine ΔT, T_g, and

the apparent solidus and liquidus temperatures, T_s and T_l respectively. Continuous cooling experiments were conducted in an rf-heating device, and the samples were heated inside graphite crucibles. Initially, samples with a mass of approximately 200 mg were inductively heated in a titanium-gettered argon atmosphere to 1225 K for 150 s. They were then cooled under the control of a proportional integral differential software algorithm at various rates. The experimental setup used for the continuous cooling rate measurements is detailed in Ref. [8].

3.2 Results

Fig. 3.1 shows some representative results of a series of continuous cooling measurements which were used to determine the critical cooling rate directly. The data were obtained by differentiating the digitally recorded temperature-time profiles measured for Vit1b. For each measurement, the sample was cooled at a controlled rate from its initial temperature to some temperature below the glass transition. In Fig. 3.1, crystallization in the sample during cooling manifests as an abrupt decrease in the magnitude of the cooling rate due to a release of the heat of fusion, as shown in the curves labeled (a), (b), and (c). The size of the crystallization peak decreases as the cooling rate magnitude increases in each subsequent measurement, and a crystallization event becomes undetectable, i.e., the sample has been rendered amorphous for the purposes of this study, after the cooling rate exceeds a certain value. Curve (d) represents such a measurement. Variations in cooling rate prior to crystallization can be attributed to limitations in the control algorithm used to modulate power during

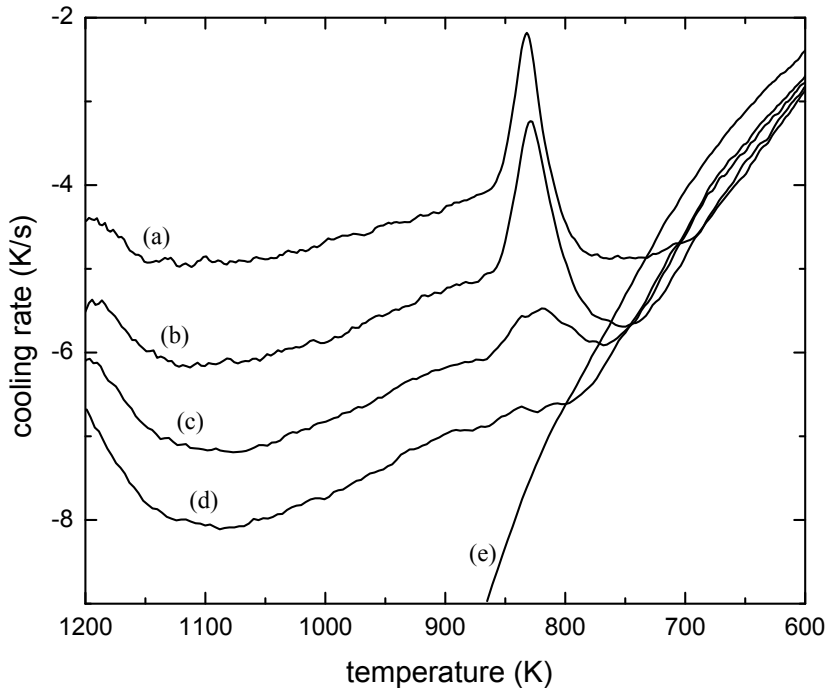

Figure 3.1: Cooling rate vs. temperature for Vit1b. The curves were obtained by differentiating the temperature-time profile recorded during cooling.

cooling. Thus, to determine a cooling rate value for each measurement, an average of the rate between 1200 K and 900 K was calculated.

Also shown in Fig. 3.1 are data taken while free-cooling the sample from its initial temperature. The curve labeled (e) illustrates another limitation of the experimental apparatus; as the temperature decreases, the maximum constant cooling rate that can be maintained decreases dramatically because the rate of heat loss from the crucible exterior limits the overall cooling rate of the sample/crucible combination. Therefore, as the constant cooling rate measurements approach the temperature where they intersect the free-cooling curve, they begin to follow the latter. In order to take measurements of cooling rates in excess of 10 K/s for Vit1c and Vit4, samples were

cooled with a flow of ultra high purity argon. Only the downstream pressure could be varied to produce different cooling rates for samples of these alloys, and estimates of R_c have greater error as a result.

Fig. 3.2 and Fig. 3.3 show the results of DTA heating scans of each alloy, used to examine crystallization and melting behavior. The arrows in Fig. 3.2 mark the onset temperature for both the glass transition and the first crystallization event. For all seven alloy compositions, the glass transition temperature remains essentially constant, with an average value of 625 K. Because the magnitude of the heat release due to crystallization was so large for Vit1b and Vit1c, the heat flow signals for these alloys have been truncated for clarity. From Fig. 3.3, it is apparent that the solidus temperature fluctuates to some degree, but T_l changes by a much greater amount between Vit1 and Vit4, reaching a maximum of 1239 K in Vit1c. In addition, the value of T_l determined for Vit1, 996 K, agrees well with previous results [9]. The liquidus temperature estimate for each alloy in the series is marked in Fig. 3.3 by an arrow, and the dashed curve has been added to illustrate the general trend in liquidus temperature from Vit1(-b) to Vit1b. It is important to note that such dramatic sensitivity of the liquidus temperature to composition is typical of alloys which lie near deep eutectics in a multicomponent phase diagram. Table 3.1 summarizes T_g, T_s, and T_l values measured from DTA, as well as ΔT and T_{rg} values derived from them.

The relationship between the experimentally determined ΔT, T_{rg}, and R_c values is shown for all the alloys in Fig. 3.4. T_{rg}, the reduced glass transition temperature, was

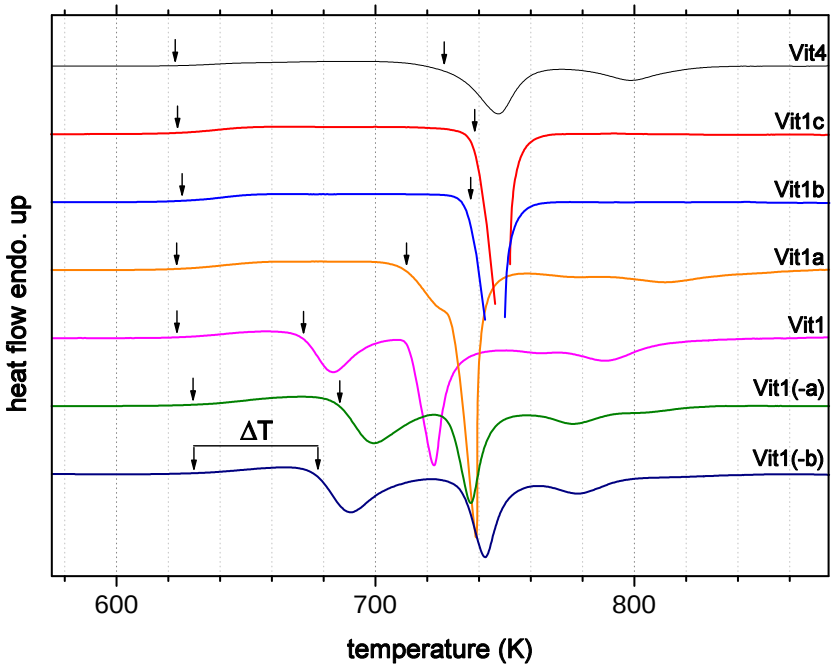

Figure 3.2: Low temperature DTA data for the alloy series.

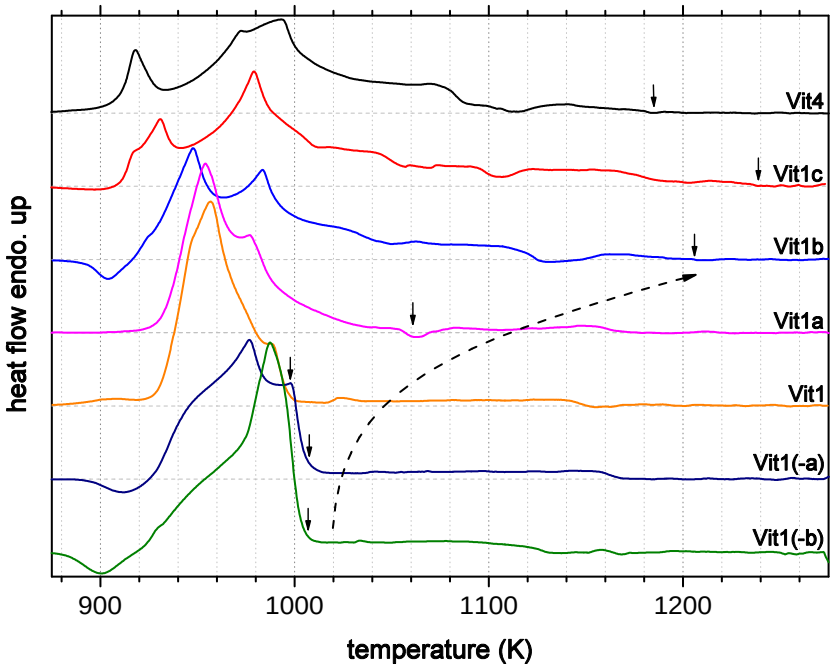

Figure 3.3: High temperature DTA data for the alloy series.

	T_g (K)	ΔT (K)	T_s (K)	T_l (K)	T_{rg}
Vit1(-b)	630	48	921	1003	0.628
Vit1(-a)	629	57	928	1006	0.625
Vit1	623	49	932	996	0.626
Vit1a	623	89	933	1057	0.589
Vit1b	625	114	917	1206	0.518
Vit1c	623	117	911	1239	0.503
Vit4	622	105	909	1185	0.525

Table 3.1: DTA results at 10K/min for the alloy series (Vit1(-b) to Vit4).

calculated using T_g/T_l. As shown in the top portion of Fig. 3.4, ΔT and T_{rg} exhibit a negative correlation as a function of composition. Both values remain fairly constant for Vit1(-b) through Vit1 but change dramatically from Vit1a to Vit4, reaching a maximum in ΔT and a minimum in T_{rg} at Vit1c. Since T_g does not vary significantly between the seven alloys studied, this means that as ΔT increases, T_l increases as well in this alloy series.

The R_c values depicted in the lower portion of Fig. 3.4 show a different behavior. At one extreme, they approach a limit of approximately 1.4 K/s in Vit1(-b) and Vit1(-a), but from Vit1a to Vit4 they increase steadily, reaching a maximum of 28 K/s in Vit4. The increase in R_c from Vit1a to Vit1c follows the trend toward smaller values of T_{rg}. The GFA of these alloys, however, does not seem to correlate well with the width of the supercooled liquid region, ΔT. As the critical cooling rate increases in this alloy series, the width of the supercooled liquid region also increases; those glass compositions with the largest ΔT are actually the poorest glass formers.

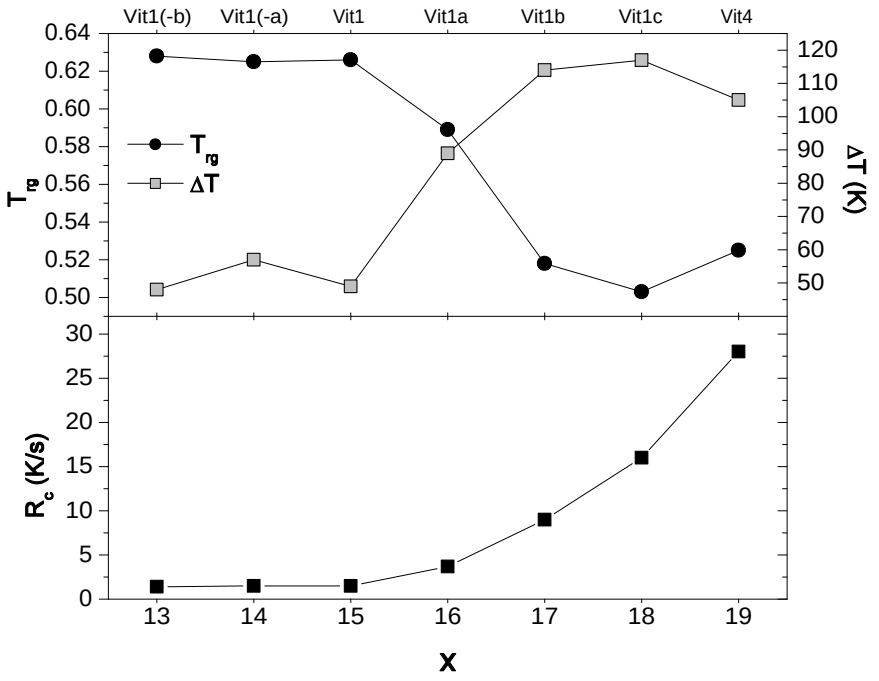

Figure 3.4: T_{rg} and ΔT as a function of alloy composition (top graph), and critical cooling rate R_c as a function of alloy composition (bottom graph). x is a parameter which describes the Vit1-Vit4 alloy series through the equation $(\mathrm{Zr}_{37.5+2.5x}\mathrm{Ti}_{62.5-2.5x})_{55}(\mathrm{Cu}_{100-3x}\mathrm{Ni}_{3x})_{41.25-1.25x}\mathrm{Be}_{3.75+1.25x}$, from $x = 13$ to $x = 19$.

3.3 Summary of Constant Cooling and Heating Experiments

The results tend to confirm Turnbull's criterion, which predicts that glass forming ability should decrease with decreasing reduced glass transition temperature. However, contrary to current understanding, the thermal stability and GFA do not show a positive correlation for the alloy series examined in this study. This suggests that different mechanisms influence crystallization upon heating and upon cooling.

It has been demonstrated that decomposition in Vit1 influences the nucleation and growth of crystalline phases in the alloy. Small-angle neutron scattering (SANS) research on Vit1a-Vit4 has also revealed the existence of spatially correlated inhomogeneities in some of these alloys after annealing [6]. This research has resulted in the determination of an effective critical temperature, T_c, for Vit1, Vit1a, and Vit1b, and has established that T_c decreases from Vit1 to Vit1c, eventually reaching the glass transition temperature between Vit1c and Vit4. Below this critical temperature, small composition fluctuations within the originally homogeneous alloy become thermodynamically favorable, and the alloy will undergo phase separation followed by crystallization. The influence of phase separation on the thermal stability and crystallization behavior near T_g will be examined in more detail in subsequent chapters.

References

[1] Z. P. Lu, H. Tan, Y. Li, and S. C. Ng. *Scripta Mater.*, 42:667–673, 2000.

[2] R. Busch, S. Schneider, A. Peker, and W. L. Johnson. *Appl. Phys. Lett.*, 67:1544, 1995.

[3] S. Schneider, P. Thiyagarajan, and W. L. Johnson. *Appl. Phys. Lett.*, 68:493, 1996.

[4] W. H. Wang, Q. Wei, S. Friedrich, M.-P. Macht, N. Wanderka, and H. Wollenberger. *Appl. Phys. Lett.*, 71:1053, 1997.

[5] J. Schroers, R. Busch, and W. L. Johnson. *Appl. Phys. Lett.*, 76:2343, 2000.

[6] J. F. Loffler, P. Thiyagarajan, and W. L. Johnson. *Mater. Trans. JIM*, 41:1530, 2000.

[7] J. Schroers, A. Masuhr, R. Busch, and W. L. Johnson. *Phys. Rev. B*, 60:11855, 1999.

[8] Schroer.

[9] R. Busch, Y. J. Kim, and W. L. Johnson. *J. Appl. Phys.*, 77:4039, 1995.

Chapter 4

Thermal Analysis: Isothermal

In order to quantify the effect of composition changes on crystallization in the Vit1(-b) to Vit4 series, a series of isothermal crystallization experiments were performed. These experiments were used to determine time-temperature-transformation (TTT) diagrams for the alloys in the series, revealing dominant trends in crystallization behavior. Additional thermal analysis was used to assess the amorphous material remaining in alloy samples following isothermal crystallization events, and x-ray diffraction (XRD) was employed to examine the crystalline content at various stages during annealing.

4.1 Setup and Technique

Fully amorphous samples of Vit1(-b), Vit1(-a), Vit1, Vit1a, Vit1b, Vit1c, and Vit4, prepared in the same manner as previous experiments, were studied using a Perkin Elmer DSC 7. Isothermal crystallization studies were performed on material that was heated from room temperature to the annealing temperature at a rate of 200 K/min. After holding samples at the annealing temperature for a specified length of time, they

were cooled to room temperature at 200 K/min. In order to determine the volume fraction crystallized during the isothermal step, subsequent DSC measurements using a constant heating rate of 40 K/min were also performed on some of the samples.

XRD data were acquired using a Co-Kα source and an INEL CPS-120 position sensitive detector. The 2θ values for each diffractogram were calibrated using the peaks of LaB_6 reference material. Following isothermal annealing and prior to XRD, samples were cooled and lightly sanded using 1200 grit sandpaper in order to remove all traces of surface oxidation.

4.2 Results

Fig. 4.1 shows representative isothermal DSC thermograms of Vit1a. The lowest temperature measurement, taken at 683 K, reveals two sluggish exothermic crystallization events whose peaks are separated by approximately 2300 seconds. As the annealing temperature is increased to 713 K (Fig. 4.1b), the spacing in time between successive crystallization events decreases and each crystallization event itself occurs more rapidly, until only one rapid crystallization event is apparent (Fig. 4.1c) at high temperatures.

Summaries of the isothermal crystallization studies are shown in Fig. 4.2 as time-temperature-transformation diagrams. For a given temperature, each TTT diagram shows the time to reach the onset (open squares) and end (filled squares) of the first crystallization event and the time to reach the onset (open squares) and end (filled squares) of the second crystallization event for each alloy. Two general trends are

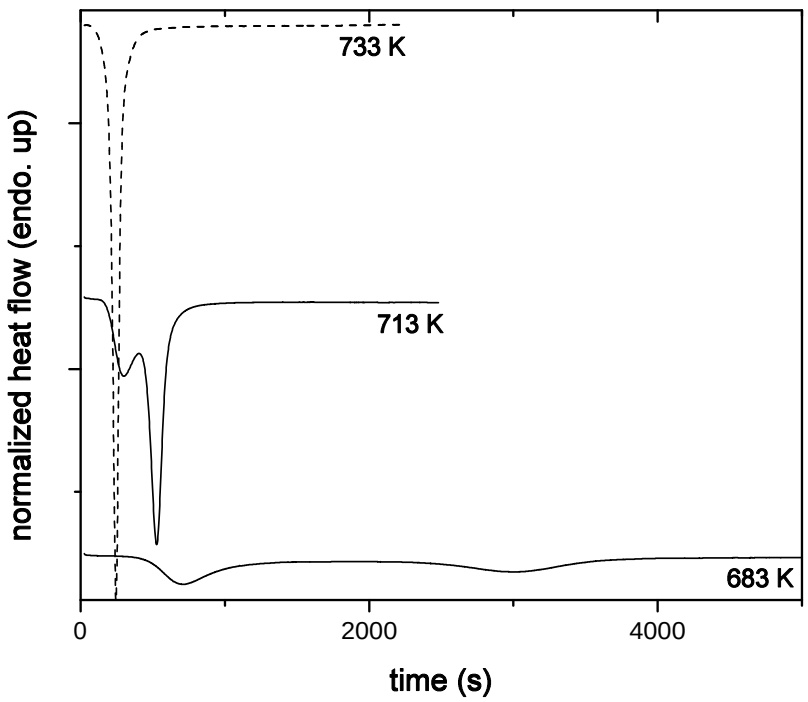

Figure 4.1: DSC thermograms of isothermal crystallization of Vit1a at 683, 713, and 733 K.

immediately apparent. First, when annealed at high temperatures, most of the alloys crystallize in one rapid event, but all the alloys crystallize in two separate events when annealed at lower temperatures. Second, isothermal stability (the time to reach crystallization) at temperatures near T_g tends to increase as the tie-line is traversed from Vit1(-b) to Vit4.

As shown in Fig. 4.1 for Vit1a, the first crystallization event for all the alloys ceases to be apparent above a certain temperature; with increasing annealing temperature, the second crystallization event steadily increases in magnitude and rate, eventually dominating the crystallization of the alloy. The temperature at which the crystallization behavior changes varies from 663 K in Vit4 to 733 K in Vit1, while two crystallization events are always evident for Vit1(-a) and Vit1(-b).

In addition to the transition from one to two crystallization events, there is also a dramatic extension of the onset of the first crystallization event to longer times between 673 and 643 K for each successive alloy in the series. This increase in isothermal stability is particularly noticeable in Vit1b, Vit1c, and Vit4, with the latter requiring annealing times on the order of 5 hours at 643 K before crystallization sets in. It should be noted that for temperatures below 643 K, long duration heat releases due to crystallization are too small in magnitude to enable accurate determination of onset and end times from DSC data for all the studied alloys. Also, because at high temperatures there is an asymmetry in crystallization behavior during heating vs. during cooling, it was not possible to acquire TTT data above the effective "nose" of the diagram for each alloy using isothermal annealing. The DSC used is limited to

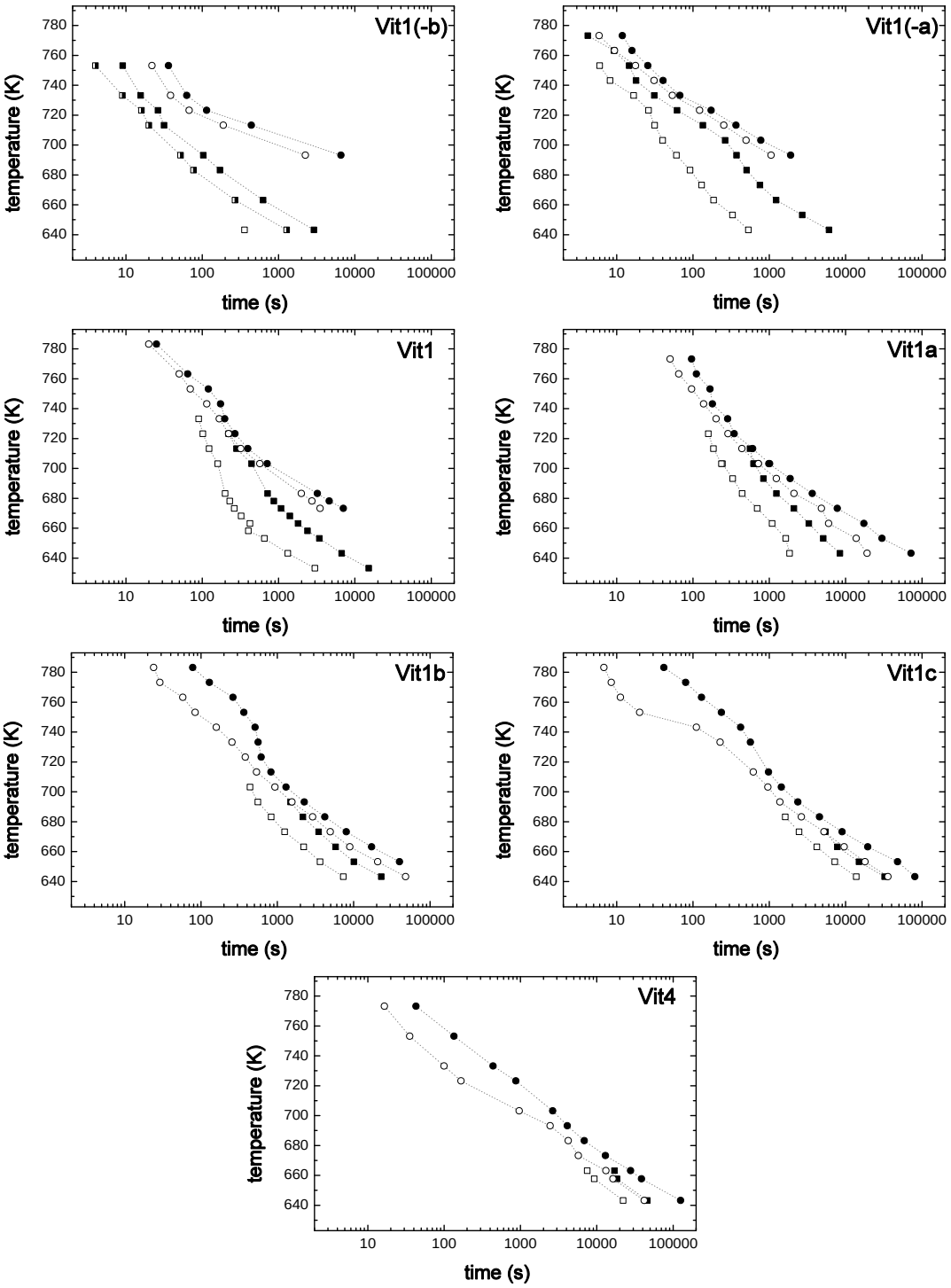

Figure 4.2: TTT diagrams measured after heating from the amorphous state for the Vit1(-b)-Vit4 series. For Vit1(-b), the time to the first peak in the heat flow signal, rather than the onset, is shown as half-filled squares.

a maximum heating rate of 3.33 K/s, and it has been shown that a heating rate of approximately 200 K/s is necessary to avoid crystallization upon heating [1].

Following the isothermal anneals, constant heating rate measurements were performed on the samples to determine whether they were completely crystalline. Surprisingly, all the alloys showed some remaining amorphous fraction after isothermal annealing, regardless of annealing temperature. By comparing the heat release during crystallization in these subsequent constant heating rate thermograms with the total heat release detected during constant heating of the as-cast material, the relative volume fraction crystallized during each step was determined and the amount of amorphous material remaining after the isothermal step was thus estimated. The results of these measurements, shown in Fig. 4.3, reveal a steady increase in volume fraction crystallized during the isothermal step as annealing temperature is increased for all the alloys except Vit4. The latter shows a crystallized volume fraction which remains fairly constant with annealing temperature.

To investigate compositional changes in the amorphous material remaining after isothermal annealing, T_g was determined for each alloy as well. Fig. 4.4 shows T_g onset values derived from constant heating rate measurements of samples after they have been processed at different isothermal annealing temperatures. Because each sample is already partially crystallized before the constant heating rate measurement used to measure T_g, the endothermic heat flow signal during the glass transition is smaller in magnitude and it is more difficult to determine the onset, resulting in the substantial scatter shown for all the alloys. In addition, because the samples have

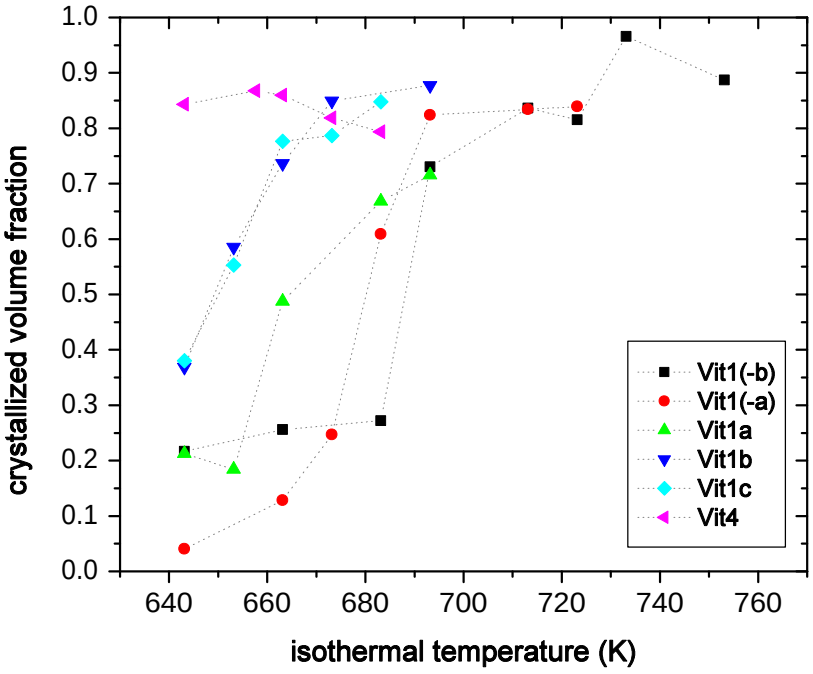

Figure 4.3: Crystallized volume fraction vs. isothermal annealing temperature for Vit1(-b)-Vit4.

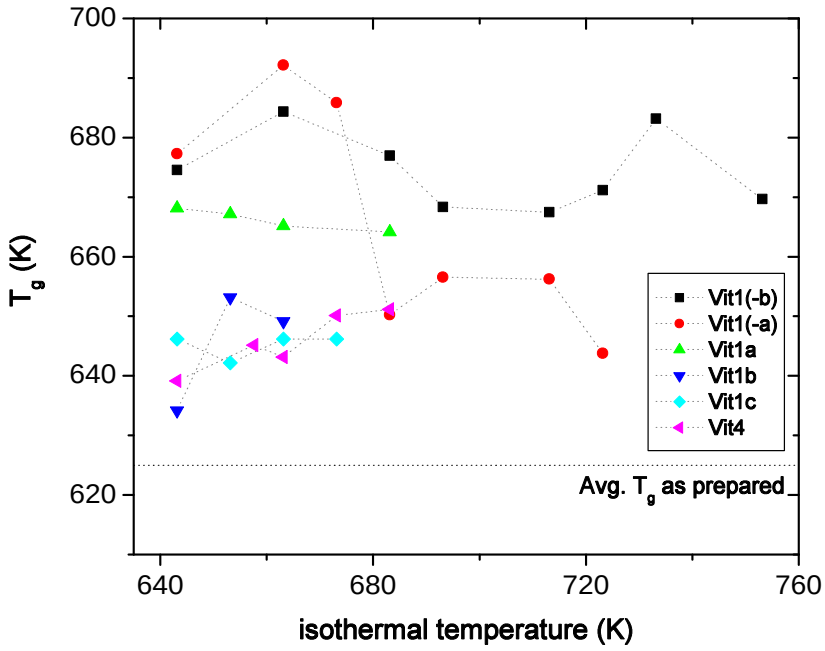

Figure 4.4: Glass transition temperature T_g of annealed and partially crystallized samples vs. isothermal annealing temperature. The horizontal dotted line represents the average T_g measured from as-cast samples.

been heated above T_g, no annealing effects due to a change in free volume should be observable, and changes in T_g can be attributed to compositional changes only. Despite the scatter, it is clear that T_g, measured subsequent to isothermal anneals on partially crystallized samples, increases substantially compared to the initially fully amorphous material. As-cast samples, in contrast, all have similar T_g values.

In order to gain some insight into the nature of the phases formed during isothermal annealing, X-ray scans were performed on samples of Vit1-Vit4. These scans are shown in Fig. 4.5a-Fig. 4.5e. Prior to the XRD measurements, samples of each alloy were held at higher annealing temperatures where only one crystallization event exists

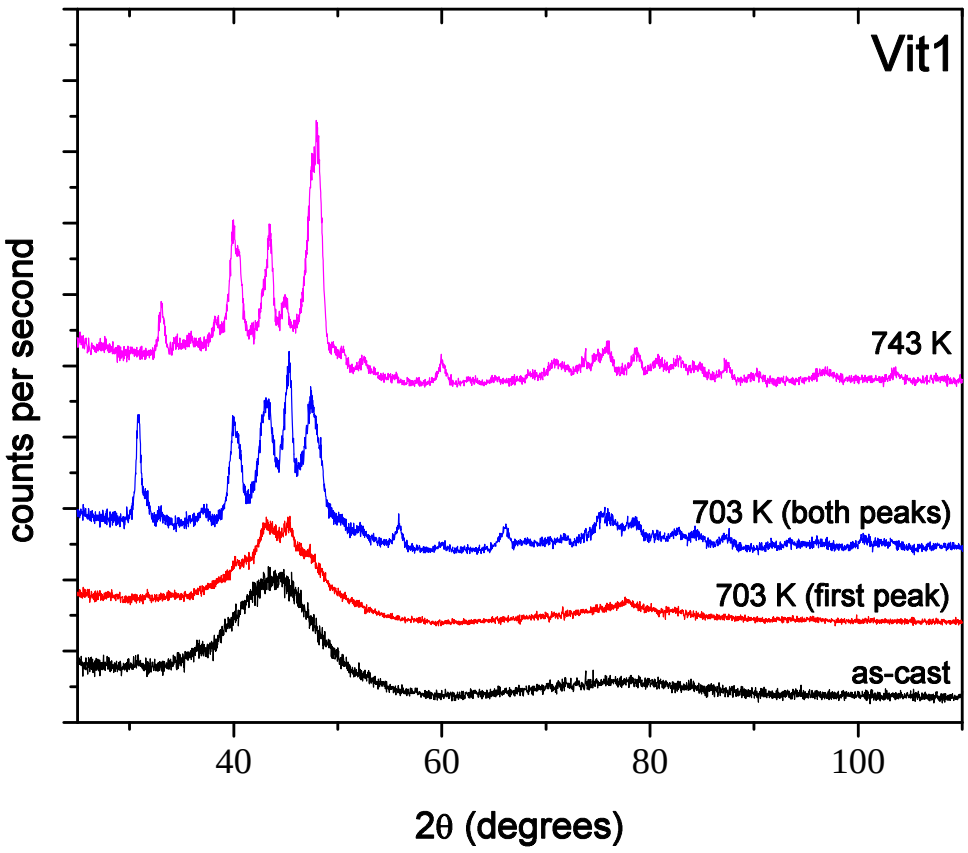

Figure 4.5: XRD spectra for Vit1 in the as-cast condition and also after isothermal anneals at two temperatures.

(see Fig. 4.2) and were quenched to room temperature after the exothermic event was complete. In addition, samples of each alloy were also annealed at low temperatures where two crystallization peaks are evident and were quenched after the first peak and after the second peak. For these, XRD data were gathered immediately after the primary crystallization and also after both primary and secondary crystallization peaks were finished.

After primary crystallization during annealing at 703 K for Vit1, 693 K for Vit1a,

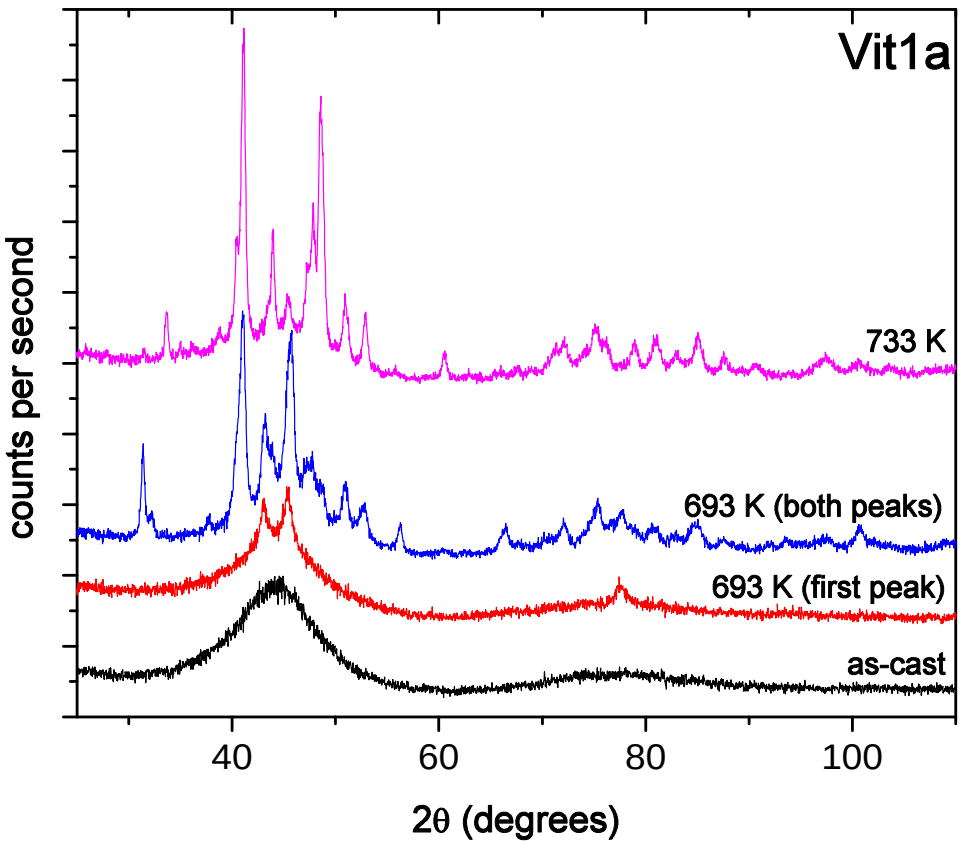

Figure 4.6: XRD spectra for Vit1a in the as-cast condition and also after isothermal anneals at two temperatures.

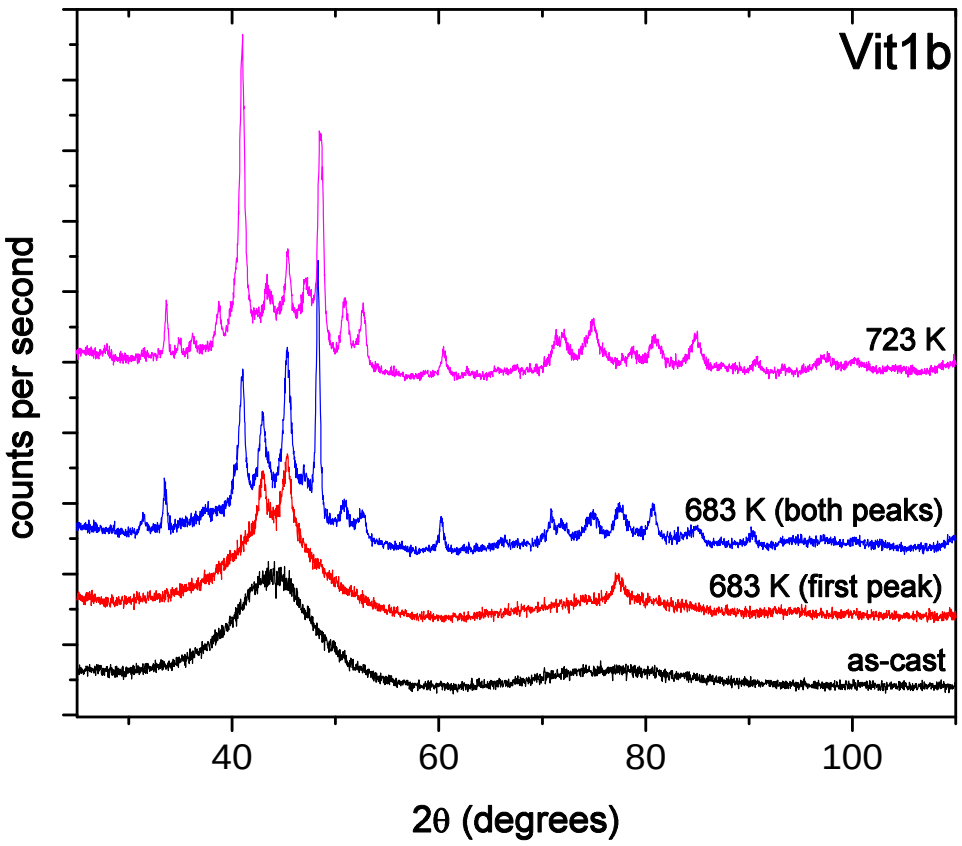

Figure 4.7: XRD spectra for Vit1b in the as-cast condition and also after isothermal anneals at two temperatures.

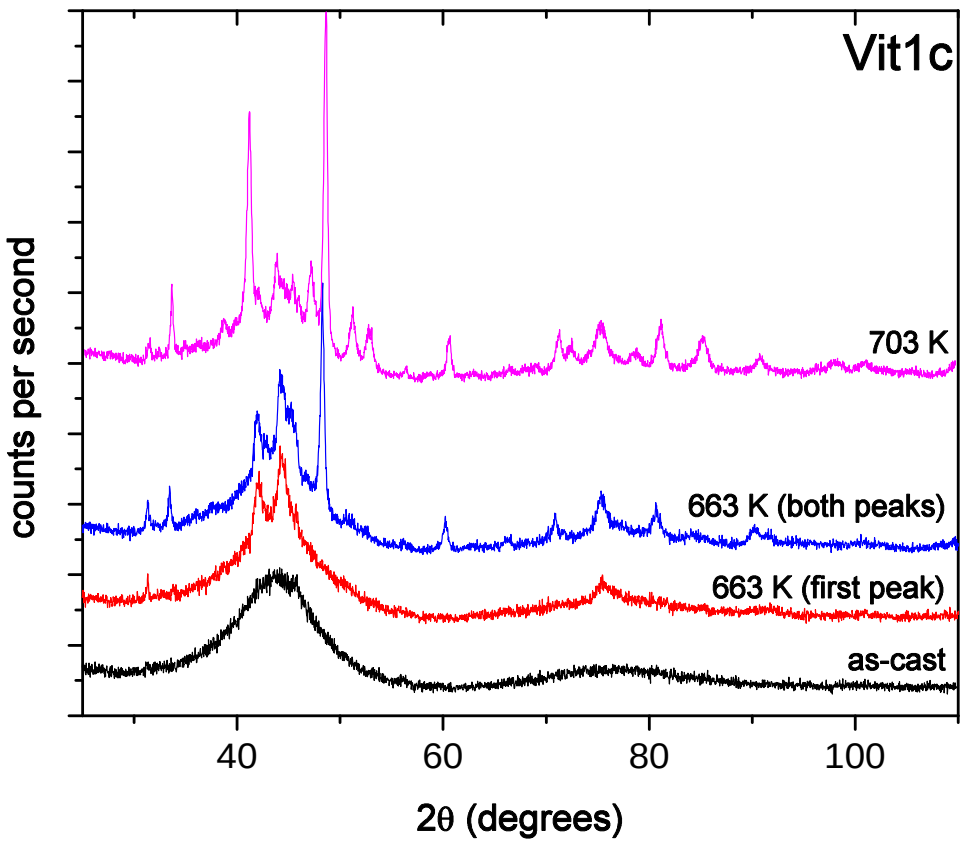

Figure 4.8: XRD spectra for Vit1c in the as-cast condition and also after isothermal anneals at two temperatures.

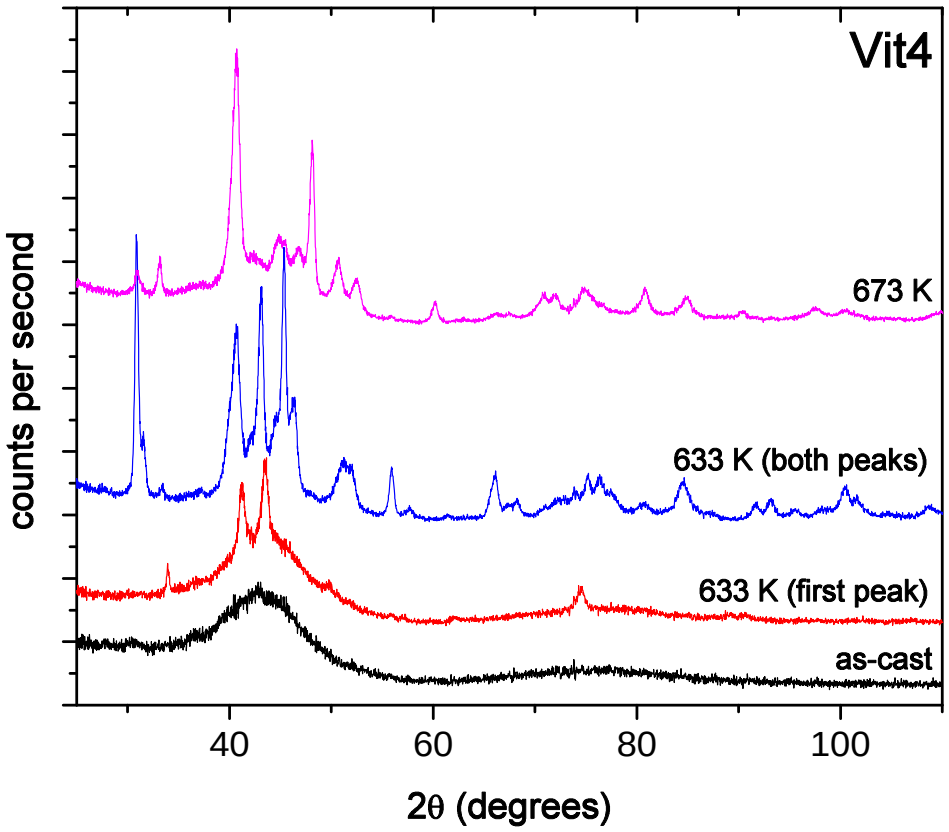

Figure 4.9: XRD spectra for Vit4 in the as-cast condition and also after isothermal anneals at two temperatures.

683 K for Vit1b, 663 K for Vit1c, and 633 K for Vit4, all the alloys show a pattern containing three peaks at approximate *d*-spacings of 2.4 Å, 2.3 Å, and 1.4 Å ($2\theta \approx 43°$, 45°, and 77°), indicating the presence of a quasicrystalline phase. This phase has been observed in other studies of Vit4 [2]. Previous evidence pointing to the existence of this phase in Zr-based BMG alloys includes XRD studies, in which the main peaks attributable to the quasicrystalline phase were indexed [3], and high-resolution TEM analysis, in which five-fold symmetry could be directly observed in micrographs. TEM studies using selected-area electron diffraction have also documented multiple zone axes corresponding to the icosahedral structure of this phase, which appears to form on the nanoscale (the quasicrystals are less than 100 nm in size) and has a quasilattice constant of 4.779 Å [2, 4]. It has been shown that the formation of quasicrystalline phases upon devitrification is common in Zr-based metallic glasses, possibly due to substantial icosahedral order existing in the supercooled liquid prior to crystallization [5]. After both crystallization events have finished during low temperature annealing of the three alloys, XRD data exhibit a large number of peaks which result from the presence of Be_2Zr, Zr_2Cu and other phases, as has been shown in previous studies [6]. Though peaks at positions corresponding to the quasicrystalline phase are still present as well, it cannot be unambiguously determined whether the quasicrystalline phase remains after the second crystallization event. There is a difference between the alloys in the types of phases that form after the second crystallization event, however. For example, whereas the peaks at d =2.6 Å, d =2.1 Å, and d =2.0 Å are present in both Vit1a and Vit1b, they are absent or exist only as a shoulder in Vit1c. In

addition, the peaks at d =3.1 Å and d =1.8 Å are present in Vit1b and Vit1c but not in Vit1a. Thus there must be at least two additional phases forming during the second crystallization event, and both of these phases are not necessarily present in each alloy. In contrast, the x-ray measurements taken at high temperatures, where only one crystallization peak is evident, show similar phases for all three alloys, with the x-ray peaks differing mainly in intensity.

4.3 Summary of Isothermal Experiments

The isothermal crystallization studies reveal the lower part of the TTT diagram for each of the investigated alloys. All alloys show evidence of a bifurcation in the crystallization behavior, and a clear trend in crystallization kinetics can be discerned from Fig. 4.2. Following the tie-line in composition space from Vit1(-b) to Vit4, one observes that the primary phase forms fairly early (<1000 seconds between 643 and 773 K) for Vit1(-b), Vit1(-a), and Vit1. Thus, relative to the rest of the series, these three alloys exhibit decreased resistance to crystallization and therefore decreased isothermal stability. For all the alloys, crystallization occurs in several steps. Following the primary crystallization event, a substantial slowdown in kinetics is observed, and the second crystallization event occurs at a much later time. In addition, the secondary event appears to dominate the crystallization of the entire sample above some temperature for each alloy, implying a competition between the primary phase and the phases formed during the second event.

The combined DSC and XRD results show that crystallization proceeds through

multiple pathways which depend on annealing temperature. At low temperatures, all the alloys first form a quasicrystalline phase. It has been postulated that this metastable phase eventually transforms to one or more new phases after a sufficient amount of annealing time at a given temperature [2, 7]. After the primary crystallization, a second crystallization process produces the remainder of the peaks observed in XRD. Whereas at low temperatures the phases that appear after the formation of the quasicrystals seem to vary somewhat between the alloys, at high temperatures all the alloys appear to crystallize very rapidly, forming a similar distribution of phases. Differences in samples crystallized at low temperature might thus be attributed to differing rates of development of the various phases and possibly also to the appearance and transformation of metastable phases during annealing. At a sufficiently high temperature which varies for each alloy, the quasicrystalline phase cannot form. Each alloy crystallizes in one rapid event above this temperature, and the consistency of the high temperature XRD results from all the alloys means that they probably represent an equilibrium distribution of crystalline phases common to the Zr-Ti-Cu-Ni-Be system.

References

[1] J. Schroers, A. Masuhr, R. Busch, and W. L. Johnson. *Phys. Rev. B*, 60:11855, 1999.

[2] N. Wanderka, M.-P. Macht, M. Seidel, S. Mechler, K. Stahl, and J. Z. Jiang. *Appl. Phys. Lett.*, 77:3935, 2000.

[3] N. Wanderka, U. Czubayko, P. Schubert-Bischoff, and M.-P. Macht. *Mater. Sci. Eng.*, A270:44, 1999.

[4] B. Van de Moortele, T. Epicier, J. L. Soubeyroux, and J. M. Pelletier. *Phil. Mag. Lett.*, 84(4):245–256, 2004.

[5] K. F. Kelton. *J. Non-Cryst. Solids*, 334-335:253–258, 2004.

[6] Q. Wei, N. Wanderka, P. Schubert-Bischoff, M.-P. Macht, and S. Friedrich. *J. Mater. Res.*, 15:1729, 2000.

[7] M.-P. Macht, S. Mechler, M. Muller, and N. Wanderka. *Mater. Sci. Forum*, 386-388:99, 2002.

Chapter 5

Discussion of the Crystallization Process in the Vit(-b)-Vit4 Alloy Series

5.1 R_c and ΔT, and Their Influence on TTT Behavior

Both the constant heating rate DTA experiments and the isothermal DSC experiments detailed in previous chapters describe an alloy series in which thermal stability increases dramatically with composition. To some extent, the constant heating rate results are analogous to traversing the TTT diagrams in a linear fashion. When cooled slowly from the melt, however, the alloys in this system typically crystallize at a temperature substantially higher than the highest temperature measured in Fig. 4.2. Consequently, the high temperature crystallization behavior (above the isothermal annealing temperature at which crystallization is most rapid) for the Vit1(-b)-Vit4 alloy series has also been explored. Measurements revealed that R_c is lowest for Vit1(-b)-Vit1, i.e. these alloys are the best glass formers in the series. R_c steadily increases,

however, from Vit1a to Vit4, reaching a maximum of approximately 27 K/s in the latter.

Because both the nucleation rate and the growth rate of crystalline phases strongly depend on the kinetics in a material, it is important to examine the extent to which viscosity plays a role in the crystallization behavior of the alloy series. As shown in Fig. 2.10, the three intermediate alloys have similar equilibrium viscosities between 590 and 655 K, and Vit1c exhibits the second lowest equilibrium viscosity in this temperature range. VFT fits to the data have yielded D^* values of 18.5, 21.3, 18.9, and 25.9 for Vit1, Vit1a, Vit1b, and Vit1c, respectively. Similar viscosity experiments conducted previously have determined a D^* value of 22.7 for Vit4 [1]. From the viscosity behavior alone, it appears that Vit4 should demonstrate the highest crystallization rate, and its thermal stability should therefore be greatly reduced. However, both Vit4 and Vit1c show the longest times until the first crystallization event within the temperature range of 643 K to 713 K.

Using the results of crystallization experiments both above and below the "nose" of the TTT diagram, some observations can be made about the dominant trends in this alloy series. Though Vit1 represents one of the best glass formers, its thermal stability is substantially reduced compared to Vit1a-Vit4. Conversely, Vit4 exhibits the highest thermal stability at low temperatures, yet its GFA is greatly reduced. In order to help explain this apparent contradiction, an estimate of the complete TTT diagram for each of the alloys has been made, taking into account the results from Fig. 4.2 and measurements of R_c. This is shown in Fig. 5.1. In this diagram,

an attempt has been made to show the interplay between GFA, represented by the shortest time to crystallization in the upper part of the TTT diagram, and thermal stability, represented by the time to crystallization at low temperatures near the glass transition. As can be seen in Fig. 5.1, Vit1(-b)-Vit1 all have low R_c values, resulting in a TTT nose which is extended to longer times (on the order of 100 s). The low temperature portion of the TTT diagram varies between these alloys, however, with the onset of crystallization pushed to earlier times in Vit1(-b) and Vit1(-a), indicating substantially reduced thermal stability. From Vit1a to Vit4, there is a smooth and continuous evolution in the shape of the TTT diagram. The nose for each subsequent alloy begins at earlier times, mirroring the increase in R_c, while at the same time the onset of crystallization for temperatures below the nose extends to longer times as the thermal stability increases. It is obvious from this diagram that a low critical cooling rate does not necessarily imply a high thermal stability in bulk glass forming compositions; completely different crystallization mechanisms operate in the high and low temperature regimes.

5.2 Effects of Decomposition

For most of the series, it has been found that there exists a decomposition process in the liquid prior to crystallization. It is likely that the incubation time preceding quasicrystal formation at low temperatures is directly influenced by such a process. As it has been suggested in several investigations that decomposition is the rate limiting step for crystallization [2, 3], increases in isothermal stability from Vit1(-b)

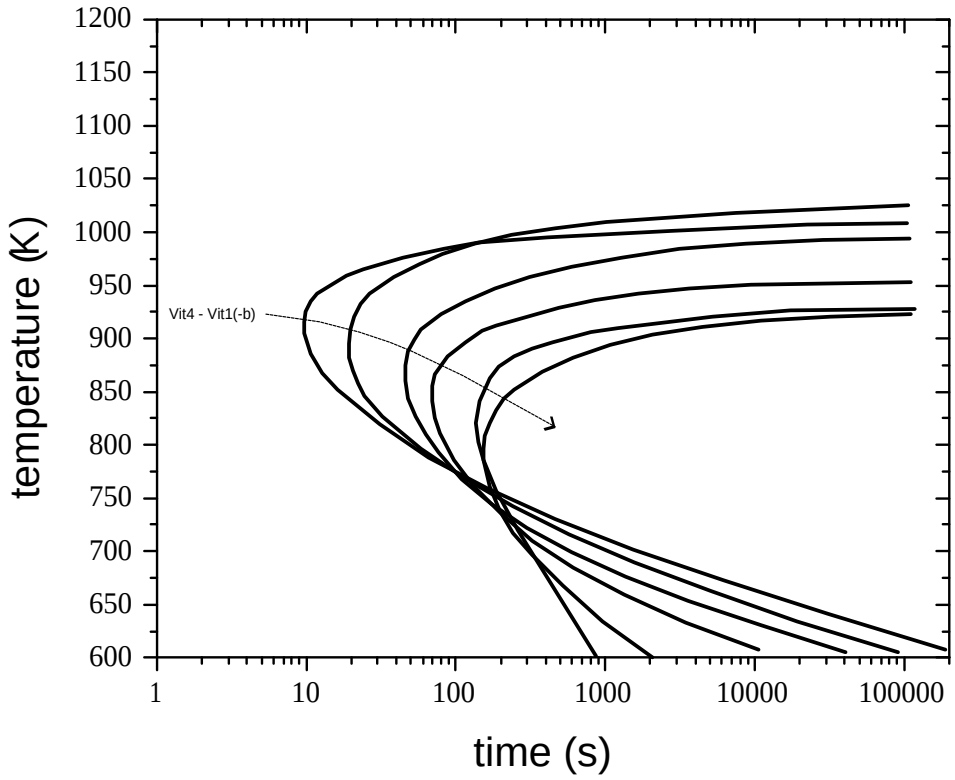

Figure 5.1: Estimates of the TTT diagrams for Vit1(-b)-Vit4, based on the results detailed in this study. Upon traversing the series from Vit1(-b)-Vit4, there is a steady extension of the nose to shorter times while at the same time there is an increase in the time to crystallization at low temperatures.

to Vit4 could therefore be attributed to differences in the timescale for decomposition for each alloy. Löffler, et al., demonstrated the existence of spatially correlated inhomogeneities in Vit1-Vit4 after annealing at various temperatures [4]. Critical temperatures, below which decomposition occurs, were reported to be 670 K, 649 K, and 642 K for Vit1, Vit1a, and Vit1b respectively. In addition, an interference maximum resulting from the existence of spatially correlated inhomogeneities was found only at 623 K for Vit1c, and none was observed for Vit4 in the temperature range studied. Fig. 5.2 compares the measured critical temperatures with T_g and crystallization onset temperatures measured via DSC at 20 K/min. Though the T_g values in these alloys vary depending on the heating rate used for measurements, it is clear from Fig. 5.2 that the critical temperature approaches the glass transition temperature as the tie line is traversed from Vit1 to Vit4 (the open circles in Fig. 5.2 represent minimum estimates of the critical temperature based on personal correspondence with Dr. Löffler). T_x, the crystallization onset temperature in Fig. 5.2, mirrors the thermal stability of each alloy composition. Thus, as the critical temperature moves closer to T_g, the thermal stability begins to increase substantially after Vit1.

The measured range of critical temperatures indicates that decomposition at a given annealing temperature near T_g occurs most rapidly in Vit1, slows down steadily as the tie-line is traversed, and is negligibly slow in Vit4. Consequently, the decomposition proceeds fastest in the alloys near Vit1, causing local composition shifts throughout the liquid and reducing the barrier to crystallization in those regions

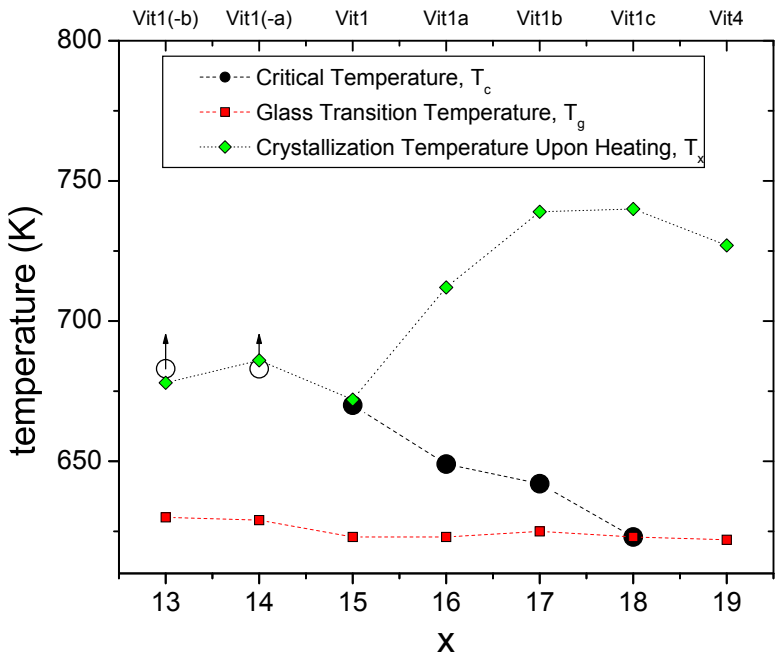

Figure 5.2: The relationship between the critical temperature for decomposition (measured by Löffler et al.) and the glass transition and crystallization onset measured via DSC at 20 K/min. x, a parameter which describes the Vit1-Vit4 alloy series, has been detailed in previous chapters.

where the composition shifts toward that of the primary phase. Though Vit1 has the most sluggish kinetics of the studied alloys, its resistance to crystallization may thus be mitigated by such composition fluctuations. Vit1c and Vit4, on the other hand, may show such dramatic increases in isothermal stability because the timescale for decomposition has been substantially increased despite their more rapid kinetics. Overall, the scenario described above predicts a crystallization process which is limited at low temperature by the rate and extent of decomposition; high temperature crystallization in these alloys, represented by the varying critical cooling rate, is not influenced by such a process.

If a decomposition process influences the formation of primary quasicrystals in this alloy series, a correlation between T_{tr} (the temperature above which crystallization ceases to occur in two steps, and thus no quasicrystallization occurs) and the critical temperature (T_c) cited above should be observable. From Fig. 2, the former temperatures are 733 K, 723 K, 703 K, 683 K, and 663 K for Vit1-Vit4, while the latter temperatures are 670 K, 649 K, 642 K, and 623 K for the first four alloys. Clearly, quasicrystals still form during isothermal annealing at temperatures well above the cited values of T_c for all the alloys. Despite the lack of agreement between these temperature values, however, it is still possible that the decomposition mechanism has some effect on crystallization above T_c. The previous SANS results reveal correlated inhomogeneities in each alloy composition below its respective T_c due to the formation of nanocrystals in phase separated domains with favorable composition. In other words, these values of T_c represent an intersection of the alloy composition

with a coherent spinodal, below which the alloy is unstable with respect to composition fluctuations and forms regularly spaced decomposed domains. At temperatures higher than the coherent spinodal but below the coherent miscibility gap, the liquid is in a metastable state, and decomposition into two chemically different supercooled liquids must overcome a nucleation barrier. In this temperature regime, decomposed regions that form will be uncorrelated in space, as will be the quasicrystals which form in those regions. Such a distribution would not be revealed by SANS. At T_{Tr}, each alloy's crystallization behavior changes abruptly because the barrier to nucleation of a phase separated domain in the supercooled liquid becomes comparable to the barrier to nucleation of the competing high temperature phase. Thus, above T_{Tr}, the primary phase which forms precludes the formation of quasicrystals and triggers a rapid series of crystallization events which manifest as one large heat release in DSC thermograms.

5.3 Compositional Considerations

The preceding discussion of the variation in crystallization kinetics among the alloys and its relation to changing decomposition kinetics has not taken into account some aspects of the polymorphic nature of the crystallization in these alloys. In order to explain how a composition fluctuation in the supercooled liquid affects crystallization, not only must the kinetics of the decomposition process be considered but also the amplitude of the composition fluctuations, where amplitude refers to the composition difference between the nominal material and the primary phase. Quasicrystals are

known to have a narrow composition (meta)stability range. At low supercoolings, the growth rate controls crystallization in Zr-based alloys [5], and it has been found that the growth rate for quasicrystalline phases depends on the chemical short range order and not the topological short range order, as the nucleation rate does [6]. The alloy with the largest composition difference between the primary quasicrystalline phase and the nominal composition should have the most sluggish crystallization kinetics. Considering this, the composition difference between the nominal glass and the primary phase might also be a crucial factor influencing the thermal stability.

Based on the experimental results detailed above, the early stages of crystallization at temperatures far below the TTT nose of each alloy in this series proceed in the following manner. After a period of time required to create a composition fluctuation in which a nucleus forms, a quasicrystalline phase appears in the supercooled liquid. This transition is non-polymorphic, and the remaining amorphous matrix has an altered composition following primary crystallization. The volume fraction that crystallizes as a quasicrystalline phase lies between 4% and 96% for the compositions and temperature ranges studied. The new matrix composition shows, on the average, an increased T_g, as revealed by constant heating rate DSC thermograms taken subsequent to the isothermal anneals. This higher T_g results from an increase in liquid density which slows down the crystallization kinetics, and the primary crystallization therefore stabilizes the glass. However, this does not necessarily mean that the GFA or thermal stability of the new composition is superior to the original composition. The thermal stability, in fact, is lower for the material containing quasicrystals, be-

cause the matrix crystallizes at a lower temperature during subsequent heating; after isothermal annealing between 643 and 653 K, Vit1a, Vit1b, Vit1c, and Vit4 show average decreases in ΔT of 61 K, 58 K, 54 K, and 50 K, respectively, compared to the as-cast material. Such a shift in crystallization temperature might be caused by the composition of the matrix shifting closer to that of a competing crystalline phase.

References

[1] R. Busch, E. Bakke, and W. L. Johnson. *Acta Mater.*, 46:4725, 1998.

[2] W. H. Wang, Q. Wei, S. Friedrich, M.-P. Macht, N. Wanderka, and H. Wollenberger. *Appl. Phys. Lett.*, 71:1053, 1997.

[3] J. Schroers, R. Busch, A. Masuhr, and W. L. Johnson. *Appl. Phys. Lett.*, 74:2806, 1999.

[4] J. F. Loffler, P. Thiyagarajan, and W. L. Johnson. *Mater. Trans. JIM*, 41:1530, 2000.

[5] J. Schroers, R. Busch, and W. L. Johnson. *Appl. Phys. Lett.*, 76:2343, 2000.

[6] J. Schroers, D. Holland-Moritz, D. M. Herlach, and K. Urban. *Phys. Rev. B*, 61:14500, 2000.

Chapter 6

Summary

This work detailed the study of various contributions to GFA in the Zr-Ti-Cu-Ni-Be alloy system. The alloy series Vit1-Vit4 was selected for analysis because all the alloys are bulk glass formers, allowing the same set of experimental techniques to be utilized for the study of each. However, because certain thermophysical properties vary substantially between the alloys, this series provided an opportunity to compare each individual influence on GFA and assess its importance. Knowledge of these influences contributes to the understanding of glass formation and can be used to predict new bulk glass forming alloys.

Equilibrium viscosity was measured in the vicinity of the glass transition using the three-point beam bending technique. Viscosity relaxation at low temperatures proceeded in two distinct steps, a phenomenon which could be attributed to a phase change occurring in each sample during annealing. All the studied alloys exhibited strong liquid behavior, reflected in their similar fragility parameter values. Their high viscosities are believed to be responsible for the overall good glass forming ability of this series. The difference in glass forming ability among the alloys, however, does not show a strong correlation with the viscosity trends.

The critical cooling rate of each alloy in the series was measured directly with a high degree of accuracy. Several influences on the kinetics of crystallization were examined using differential thermal analysis and differential scanning calorimetry, as well as x-ray diffraction. R_c increases steadily from approximately 1.4 K/s in Vit1(-b) to 28 K/s in Vit4. At the same time, the thermal stability increases dramatically between Vit1 and Vit4, while the reduced glass transition temperature drops substantially. It was found that Turnbull's criterion for glass formation, the reduced glass transition temperature, correlates well with the glass forming ability of the various alloys, and therefore is a useful criterion for characterizing GFA. The thermal stability, which is frequently used as a criterion for characterizing GFA (mainly due to the experimental challenge of measuring critical cooling rate directly), does not at all correlate with GFA. Thermal stability should not be used to predict GFA. The fact that GFA and thermal stability are not correlated can be explained by a chemical decomposition process occurring in the supercooled liquid during annealing.

Overall, the results indicate that crystallization is a complex process in this 5-component system. Local chemistry plays an important role in determining the time scales for forming crystalline nuclei at low temperatures, and the process is mitigated to some extent by composition fluctuations caused by decomposition. Thus, the difference between the nominal alloy composition and the primary phase composition, and the processes which must occur before the former approaches the latter in the supercooled liquid, primarily determine the thermal stability in this system. The GFA, on the other hand, is influenced by a different crystallization process at high

temperatures, and the reduced glass transition temperature in this series tends to reflect this.